

Exchange Coupling in Homo- and Heterodinuclear Complexes Cu^{II}M [M = Cr(III), Mn(III), Mn(II), Fe(III), Co(III), Co(II), Ni(II), Cu(II), Zn(II)]. Synthesis, Structures, and Spectroscopic Properties

Frank Birkelbach,[†] Manuela Winter,[†] Ulrich Flörke,[‡] Hans-Jürgen Haupt,[‡] Christian Butzlaff,[§] Marek Lengen,[§] Eckhard Bill,[§] Alfred X. Trautwein,[§] Karl Wieghardt,[†] and Phalguni Chaudhuri^{†*}

Anorganische Chemie I, Ruhr-Universität, D-44780 Bochum, Germany, Allgemeine Anorganische und Analytische Chemie, Universität-Gesamthochschule Paderborn, D-33098 Paderborn, Germany, and Institut für Physik, Medizinische Universität, D-23538 Lübeck, Germany

Received December 14, 1993[®]

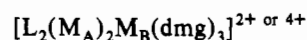
A series of heterodinuclear complexes Cu^{II}M, where M = Cr(III) (1), Mn(III) (2), Mn(II) (3), Fe(III) (4), Co(II) (5), Co(III) (6), Ni(II) (7), Cu(II) (8), and Zn(II) (9), containing the oximato dianion (Dopn²⁻) as bridging ligand and 1,4,7-trimethyl-1,4,7-triazacyclononane (L) as one of the two capping ligands have been synthesized by using the [Cu(DopnH)]⁺ cation (H₂Dopn = 3,9-dimethyl-4,8-diazaundeca-3,8-diene-2,10-dione dioxime) as a ligand for the different MLⁿ⁺ centers. The compounds have been characterized on the basis of IR, electronic, and EPR spectroscopy and variable-temperature (2–295 K) magnetic susceptibility measurements. The dinuclear complexes are quasi-isostructural with the copper(II) ion in a distorted square pyramidal environment, CuN₄O, and the M ion, except for that in 8, is six-coordinate with the MN₃O₃ or MN₃O₂Cl coordination sphere. For M = Cu (8), the coordination geometry of M with the CuN₃O₂ chromophore is also square pyramidal. The crystal and molecular structures of the compounds [(Dopn)Cu^{II}(OH₂)Cr^{III}(OCH₃)L](ClO₄)₂·H₂O (1) and [(Dopn)Cu^{II}(μ-CH₃COO)-Mn^{III}L](ClO₄)₂·2H₂O (2) have been established by X-ray diffraction. 1 crystallizes in the monoclinic system space group P2₁/n, with cell constants *a* = 13.096(3) Å, *b* = 17.933(4) Å, *c* = 15.994(3) Å, β = 113.49(3)°, *V* = 3444.9(13) Å³, and *Z* = 4. The structure consists of oximato-bridged Cu^{II}Cr^{III} dications and noncoordinated perchlorate anions, with a Cu···Cr distance of 3.86 Å. The crystal data for 2 are as follows: orthorhombic, space group P2₁2₁2₁, *a* = 12.275(4) Å, *b* = 14.171(9) Å, *c* = 19.780(3) Å, *V* = 3441(2) Å³, *Z* = 4. The structure consists of a six-coordinate Mn(III) center, MnN₃O₃, and the copper(II) center has an N₄O donor set. An acetate group bridges the manganese and copper ions with a Cu···Mn separation of 3.54 Å. A low-quality X-ray structure determination for the Cu^{II}Fe^{III} complex is also reported. Analysis of the susceptibility data yields a strong antiferromagnetic interaction (2*J* = -596 cm⁻¹) between adjacent Cu(II) ions in 8, showing once again that bridging oximes are good mediators for exchange interactions. The strength of the effective antiferromagnetic interaction decreases with increasing number of unpaired electrons in this series, 8 > 7 > 5 > 4 ~ 3. Moderately strong ferromagnetic interactions have been observed for Cu^{II}Mn^{III} (2) (2*J* = +109 cm⁻¹) and Cu^{II}Cr^{III} (1) (2*J* = +37 cm⁻¹). A qualitative rationale has been provided for the difference in magnetic behaviors. The X-band EPR spectra (3–77 K) have been measured to establish the ground states of the dinuclear complexes. Well-resolved *S* = 2 EPR spectra for different heterometal systems have been observed.

Introduction

The study of the exchange interaction^{1–4} between paramagnetic metal centers through multiatom bridges has been one of the most active research fields in coordination chemistry with the aim of understanding fundamental factors governing the magnetic properties of transition metal compounds and finding appropriate systems applicable as building units for the design of new materials. Additionally, the importance of exchange coupling in multimetal proteins⁵ has stimulated much interest in exploring the ability of bridging multiatom ligands to mediate exchange coupling in M(bridging ligand)M' systems. Both homo- and heteropoly-

metallic systems provide opportunity to study experimentally and theoretically fundamental electronic processes such as electron exchange in biological metallic sites and/or their chemical models. Metal ions assembled in such a multimetal system can exhibit magnetic properties drastically different from those of the individual ions due to electron exchange phenomena. New exchange pathways can be expected for heteropolynuclear complexes, where unusual sets of magnetic orbitals can be brought into close proximity; hence investigations of a series of heteropolynuclear complexes might be more informative in comparison to those of homopolynuclear complexes. The heteropolymetallic systems are of interest to both biologists and bioinorganic chemists investigating the structure and function of the polynuclear metal centers in proteins and to physicists or physical inorganic chemists searching for new magnetic materials.

With the aim of providing some answers to questions regarding the effectiveness of polyatomic bridging ligands like oximes and their metal complexes in propagating exchange interactions, we recently described⁶ a series of dimethylglyoximate-bridged linear heterotrinnuclear complexes of general formula



where M_A = Fe(III), Mn(III), or Mn(IV), M_B = Zn(II), Cu(II),

[†] Ruhr-Universität Bochum.

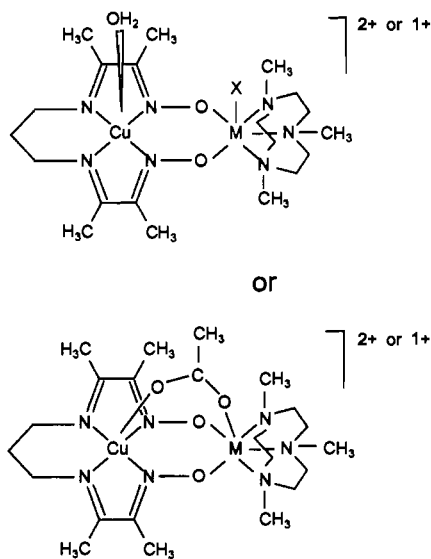
[‡] Universität-Gesamthochschule Paderborn.

[§] Medizinische Universität zu Lübeck.

[®] Abstract published in *Advance ACS Abstracts*, July 15, 1994.

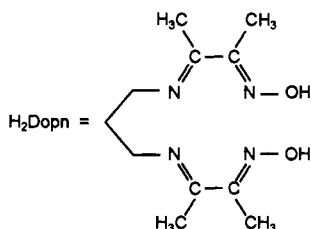
- (1) Hatfield, W. E. In *Theory and Applications of Molecular Paramagnetism*; Boudreaux, E. S., Mulay, L. N., Eds.; Wiley: New York, 1976; p 350.
- (2) Bencini, A.; Gatteschi, D. *EPR of Exchange Coupled Systems*; Springer-Verlag: Berlin, 1990.
- (3) Kahn, O. *Molecular Magnetism*; VCH Verlagsgesellschaft: Weinheim, Germany, 1993.
- (4) *Magnetic Molecular Materials*; Gatteschi, D., Kahn, O., Miller, J. S., Palacio, F., Eds.; NATO ASI Series E, Vol. 198; Kluwer Academic: Dordrecht, The Netherlands, 1990.
- (5) Solomon, E. I. In *Metal Cluster in Proteins*; Que, L., Jr., Ed.; American Chemical Society: Washington, DC, 1988; p 116.

Ni(II), Co(II), Fe(II), or Mn(II), and L represents the simple tridentate cyclic amine 1,4,7-trimethyl-1,4,7-triazacyclononane, which coordinates facially in octahedral complexes. In continuation of our earlier interest in heterobimetallic systems,⁷ we have prepared a series of compounds with the following structural motifs:



(M = Cr(III), Mn(III), Mn(II), Fe(III), Co(III), Co(II), Ni(II), Cu(II), Zn(II) and X = Cl⁻, CH₃O⁻)

This has been accomplished by using [Cu(DopnH)(OH₂)](ClO₄)^{9,10} as a ligand for a metal center. H₂Dopn stands for 3,9-dimethyl-4,8-diazaundeca-3,8-diene-2,10-dione dioxime



We report here the syntheses and magnetic and spectroscopic properties of the aforementioned compounds, together with crystal structures of the Cu^{II}Cr^{III} and Cu^{II}Mn^{III} compounds. Throughout this paper, the compounds are denoted by the metal centers only; the macrocyclic amine and the oxime ligands are omitted for simplicity.

Experimental Section

The macrocycle 1,4,7-trimethyl-1,4,7-triazacyclononane (=L) was prepared as described previously.⁸ 3,9-Dimethyl-4,8-diazaundeca-3,8-diene-2,10-dione dioxime (H₂Dopn) and its mononuclear copper(II) complex were obtained by the literature methods.^{9,10} All other starting materials were commercially available and were of reagent grade. Elemental analyses (C, H, N) were performed by the Microanalytical Laboratory, Ruhr-Universität Bochum. Copper and nickel were determined gravimetrically by using *N*-benzoyl-*N*-phenylhydroxylamine and

dimethylglyoxime, respectively. Zinc was determined by atomic absorption spectrometry. Quantitative determination of other metals was performed spectrophotometrically: chromium as chromate; iron, manganese, and cobalt as their dipicolinic acid complexes. The perchlorate anion was determined gravimetrically as tetraphenylarsonium perchlorate. Electronic absorption spectra were measured on a Perkin-Elmer Lambda 9 spectrophotometer in a methanolic solution. Fourier transform infrared spectroscopy on KBr pellets was performed on a Perkin-Elmer 1720X FT-IR instrument.

Magnetic susceptibilities of powdered samples were recorded on a SQUID magnetometer (MPMS, Quantum Design) in the temperature range 2–295 K with an applied field of 1 T. Experimental susceptibility data were corrected for the underlying diamagnetism using Pascal's constants.

The X-band EPR spectra of the polycrystalline material either as solid or in solution were recorded at various temperatures between 3 and 77 K with a Bruker ER 200 D-SRC spectrometer equipped with a standard TE 102 cavity, an Oxford Instruments liquid helium continuous-flow cryostat, an NMR gaussmeter, a frequency meter, and a data acquisition system (own development).

Syntheses of the Compounds. The synthons [Cu(DopnH)(OH₂)](ClO₄)·H₂O,⁹ LCrBr₃,⁷ and LFeCl₃¹¹ were prepared by the literature procedures.

[(Dopn)Cu^{II}(OH₂)Cr^{III}(OCH₃)L](ClO₄)₂·2H₂O (1). To a suspension of 0.46 g (1 mmol) of LCrBr₃ in 30 mL of methanol was slowly added 0.62 g of AgClO₄·H₂O (2.8 mmol) with stirring. The suspension was refluxed under argon for 0.5 h; during this time a blue-violet solution with a concomitant formation of AgBr resulted. Precipitated AgBr was filtered off, and the clear blue-violet solution was charged with a solid sample (0.4 g, 1 mmol) of [Cu(DopnH)(OH₂)]ClO₄ and 1 mL of triethylamine. The resulting red-brown solution was refluxed for 0.5 h, and NaClO₄·H₂O (0.5 g) was added. Upon standing at ambient temperature, the mixture deposited red-brown crystals. These were filtered off and air-dried. One of these crystals was used in the structural characterization of the complex reported below. Yield: 0.51 g (~66%). Anal. Calcd for [C₂₁H₄₆N₇O₅CuCr](ClO₄)₂: C, 31.88; H, 5.86; N, 12.39; Cu, 8.03; Cr, 6.57; ClO₄, 25.14. Found: C, 31.3; H, 5.7; N, 12.6; Cu, 8.3; Cr, 6.6; ClO₄, 25.3.

[(Dopn)Cu^{II}(μ-OOCCH₃)Mn^{III}L](ClO₄)₂·2H₂O (2). A solution of the cyclic amine (0.17 g, 1 mmol) in 40 mL of methanol was treated with a sample of manganese(III) acetate (0.26 g, 1 mmol) under vigorous stirring in a round-bottomed flask. After 0.25 h of stirring, the resulting red-brown solution was charged with a sample of [Cu(DopnH)(OH₂)](ClO₄) (0.44 g, 1 mmol) and with sodium methoxide (0.14 g, 2.5 mmol). The very dark solution was stirred for a further 2 h at ambient temperature, followed by an addition of NaClO₄·H₂O (0.14 g). The dark solution was filtered to remove any solid particles. The solution kept at room temperature provided deep brown (almost black) crystals. The crystals were collected by filtration and air-dried. Yield: 0.46 g (~56%). Anal. Calcd for [C₂₂H₄₆N₇O₆CuMn](ClO₄)₂: C, 32.14; H, 5.64; N, 11.93; Cu, 7.73; Mn, 6.68; ClO₄, 24.20. Found: C, 32.5; H, 5.4; N, 12.0; Cu, 7.1; Mn, 6.7; ClO₄, 24.5.

[(Dopn)Cu^{II}(μ-OOCCH₃)Mn^{III}L](PF₆)₂·2H₂O (2a). Complex 2a was obtained similarly to complex 2 with sodium hexafluorophosphate instead of sodium perchlorate used as the anion source. Dark brown crystals were obtained. Yield: 0.40 g (~44%). Anal. Calcd for [C₂₂H₄₆N₇O₆CuMn](PF₆)₂: C, 28.94; H, 5.08; N, 10.74; Cu, 6.96; Mn, 6.02. Found: C, 29.0; H, 5.20; N, 10.8; Cu, 7.3; Mn, 6.4.

[(Dopn)Cu^{II}(μ-OOCCH₃)Mn^{III}L](ClO₄) (3). All operations were done strictly under an argon atmosphere. Complex 3 was obtained as black needles in a manner similar to that for 2 using manganese(II) acetate, Mn(OAc)₂·4H₂O, instead of "Mn^{III}(OAc)₃" as the manganese source. The compound in the solid state is air-stable. Yield: 0.30 g (~42%). Anal. Calcd for [C₂₂H₄₂N₇O₄MnCu](ClO₄): C, 38.49; H, 6.17; N, 14.28; Cu, 9.26; Mn, 8.00; ClO₄, 14.49. Found: C, 38.6; H, 6.4; N, 14.0; Cu, 8.9; Mn, 8.1; ClO₄, 14.7.

[(Dopn)Cu^{II}(OH₂)Fe^{III}(Cl)L](ClO₄)₂ (4). A suspension of LFeCl₃ (0.33 g, 1 mmol) and [Cu(DopnH)(OH₂)]ClO₄ (0.44 g, 1 mmol) in water (40 mL) containing triethylamine (1 mL) was stirred at room temperature for 1 h. To the resulting clear dark brown solution was added NaClO₄·H₂O (0.5 g). After the mixture had stood at ambient temperature for 2 days, dark brown needle-shaped crystals separated from the solution. These were filtered off and air-dried. Yield: 0.62 g

- (6) (a) Chaudhuri, P.; Winter, M.; Fleischhauer, P.; Haase, W.; Flörke, U.; Haupt, H.-J. *J. Chem. Soc., Chem. Commun.* **1990**, 1728. (b) Chaudhuri, P.; Winter, M.; Della Védova, B. P. C.; Fleischhauer, P.; Haase, W.; Flörke, U.; Haupt, H.-J. *Inorg. Chem.* **1991**, *30*, 4777. (c) Chaudhuri, P.; Winter, M.; Birkelbach, F.; Fleischhauer, P.; Haase, W.; Flörke, U.; Haupt, H.-J. *Inorg. Chem.* **1991**, *30*, 4291.
 (7) See for example: Chaudhuri, P.; Winter, M.; Küppers, H.-J.; Wieghardt, K.; Nuber, B.; Weiss, J. *Inorg. Chem.* **1987**, *26*, 3302.
 (8) Wieghardt, K.; Chaudhuri, P.; Nuber, B.; Weiss, J. *Inorg. Chem.* **1982**, *21*, 3086.
 (9) Uhlig, E.; Friedrich, M. *Z. Anorg. Allg. Chem.* **1966**, *343*, 299.
 (10) Gagné, R. *J. Am. Chem. Soc.* **1976**, *88*, 6709.

- (11) Chaudhuri, P.; Winter, M.; Wieghardt, K.; Gehring, S.; Haase, W.; Nuber, B.; Weiss, J. *Inorg. Chem.* **1988**, *27*, 1564.

(~80%). Anal. Calcd for $[\text{C}_{20}\text{H}_{41}\text{N}_7\text{O}_3\text{ClCuFe}](\text{ClO}_4)_2$: C, 30.75; H, 5.29; N, 12.56; Cu, 8.13; Fe, 7.15; ClO_4 , 25.46. Found: C, 30.9; H, 5.4; N, 12.6; Cu, 7.9; Fe, 6.8; ClO_4 , 25.5.

[(Dopn)Cu^{II}(μ -OOCCH₃)Fe^{III}L](ClO₄)₂·H₂O (4a). To an aqueous solution of sodium acetate (1 g in 40 mL of H₂O) containing triethylamine (1 mL) were added LFeCl₃ (0.33 g, 1 mmol) and [Cu(DopnH)(OH₂)](ClO₄) (0.44 g, 1 mmol). The suspension was stirred at room temperature for 1 h, yielding a clear dark brown solution. Sodium perchlorate hydrate (0.5 g) was added, the solution was filtered to remove any solid particles, and the filtrate was kept at ambient temperature for 2 days. Dark brown crystals separated from the solution. These were filtered off and air-dried. Yield: 0.5 g (62%). Anal. Calcd for $[\text{C}_{22}\text{H}_{44}\text{N}_7\text{O}_5\text{FeCu}](\text{ClO}_4)_2$: C, 32.83; H, 5.51; N, 12.18; Fe, 6.94; Cu, 7.89; ClO_4 , 24.71. Found: C, 32.7; H, 5.6; N, 12.3; Fe, 7.1; Cu, 8.0; ClO_4 , 24.6.

[(Dopn)Cu^{II}(OH₂)Co^{III}(Cl)L](ClO₄) (5). All operations were performed strictly under an argon atmosphere. To a rapidly stirred and degassed solution of 1,4,7-trimethyl-1,4,7-triazacyclononane (0.085 g, 0.5 mmol) in 20 mL of water was added a sample of CoCl₂·6H₂O (0.12 g, 0.5 mmol), upon which a light blue precipitate of presumably cobaltous hydroxide appeared. A sample of [Cu(DopnH)(OH₂)](ClO₄) (0.22 g, 0.5 mmol) and 0.5 mL of triethylamine were added to the suspension under constant stirring and mild warming. Stirring was continued for 0.5 h until a nearly clear solution was obtained. The solution was filtered under argon to remove any solid particles. To the clear solution was added a degassed solution of NaClO₄·H₂O (0.8 g) in water (5 mL). After 1 h, the precipitated black-brown needles were collected and argon-dried. The dried compound in the solid state is air-stable. Yield: 0.15 g (44%). Anal. Calcd for $[\text{C}_{20}\text{H}_{41}\text{N}_7\text{O}_3\text{CuCo}(\text{Cl})](\text{ClO}_4)_2$: C, 35.07; H, 6.03; N, 14.31; ClO_4 , 14.52; Cu, 9.28; Co, 8.60. Found: C, 35.5; H, 6.0; N, 14.4; ClO_4 , 14.6; Cu, 9.2; Co, 8.5.

Compound **5a**, [(Dopn)Cu^{II}(μ -OOCCH₃)Co^{III}L](ClO₄), was obtained similarly to complex **5** with Co(OAc)₂·4H₂O as the cobalt(II) source.

[(Dopn)Cu^{II}(OH₂)Co^{III}(Cl)](ClO₄)₂ (6). Complex **6** was obtained as dark red-brown crystals in a manner similar to that for **5** in the presence of air. Yield: 0.18 g (46%). Anal. Calcd for $[\text{C}_{20}\text{H}_{41}\text{N}_7\text{O}_3\text{CuCoCl}](\text{ClO}_4)_2$: C, 29.88; H, 5.27; N, 12.50; ClO_4 , 25.36; Cu, 8.09; Co, 7.51. Found: C, 30.1; H, 5.0; N, 12.5; ClO_4 , 25.4; Cu, 8.3; Co, 7.6.

[(Dopn)Cu^{II}(OH₂)Ni^{II}L](ClO₄)₂·H₂O (7). To a solution of Ni(ClO₄)₂·6H₂O (0.18 g, 0.5 mmol) in 20 mL of water was added 0.5 mmol (0.085 g) of the cyclic amine, yielding a light blue precipitate of Ni(OH)₂. The suspension was charged with a sample of [Cu(DopnH)(OH₂)]ClO₄ (0.22 g, 0.5 mmol) and 0.5 mL of triethylamine. The mixed solution was refluxed for 20 min and hot-filtered. The cooled solution yielded within a few hours brown needles, which were filtered off and air-dried. Yield: 0.23 g (58%). Anal. Calcd for $[\text{C}_{20}\text{H}_{45}\text{N}_7\text{O}_5\text{CuNi}](\text{ClO}_4)_2$: C, 30.61; H, 5.78; N, 12.49; ClO_4 , 25.35; Cu, 8.10; Ni, 7.48. Found: C, 30.5; H, 5.7; N, 12.5; ClO_4 , 25.3; Cu, 8.2; Ni, 7.8.

Compound **7a**, [(Dopn)Cu^{II}(μ -OOCCH₃)Ni^{II}L](ClO₄), was obtained in a manner similar to that for **7** by using Ni(OAc)₂·4H₂O as the nickel source, together with 1 g of sodium acetate.

[(Dopn)Cu^{II}(OH₂)Cu^{II}L](ClO₄)₂·2H₂O (8). A 0.22 g (0.5 mmol) sample of [Cu(DopnH)(OH₂)](ClO₄) was dissolved on warming in 20 mL of water by an addition of 0.1 g of NaOH. A second solution containing Cu(ClO₄)₂·6H₂O (0.19 g, 0.5 mmol) and the cyclic amine (0.085 g, 0.5 mmol) in 5 mL of water was added to the first solution. Within a short time, brown needles precipitated and were separated by filtration and air-dried. Yield: 0.29 g (75%). Anal. Calcd for $[\text{C}_{20}\text{H}_{45}\text{N}_7\text{O}_5\text{Cu}_2](\text{ClO}_4)_2$: C, 30.42; H, 5.74; N, 12.42; ClO_4 , 25.19; Cu, 16.09. Found: C, 30.0; H, 5.7; N, 12.3; ClO_4 , 25.3; Cu, 15.8.

[(Dopn)Cu^{II}(OH₂)Zn^{II}L](ClO₄)₂·H₂O (9). Complex **9** was prepared as dark red crystals in a manner similar to that for **8** by using Zn(ClO₄)₂·6H₂O instead of Cu(ClO₄)₂ as the zinc source. Yield: 0.28 g (71%). Anal. Calcd for $[\text{C}_{20}\text{H}_{45}\text{N}_7\text{O}_5\text{CuZn}](\text{ClO}_4)_2$: C, 30.35; H, 5.73; N, 12.39; ClO_4 , 25.13; Cu, 8.03; Zn, 8.26. Found: C, 30.4; H, 5.7; N, 12.4; ClO_4 , 25.5; Cu, 8.2; Zn, 8.4.

Caution! Although we experienced no difficulties with the compounds isolated as their perchlorate salts, the unpredictable behavior of perchlorate salts necessitates extreme caution in their handling.

Crystal Structure Determinations. Diffraction data were obtained on a Siemens P4 diffractometer, using graphite-monochromatized Mo K α radiation at 293 K. Pertinent crystallographic parameters are summarized in Table 1. The data were corrected for Lorentz and polarization effects, but it was not necessary to account for crystal decay. An empirical

Table 1. Crystallographic Data for [(Dopn)Cu^{II}(OH₂)Cr^{III}(OCH₃)L](ClO₄)₂·H₂O (**1**) and [(Dopn)Cu^{II}(μ -CH₃COO)Mn^{III}L](ClO₄)₂·2H₂O (**2**)

	Cu ^{II} Cr ^{III} (1)	Cu ^{II} Mn ^{III} (2)
chem formula	C ₂₁ H ₄₆ N ₇ O ₁₃ Cl ₂ CrCu	C ₂₂ H ₄₆ N ₇ O ₁₄ Cl ₂ CuMn
fw	791.10	822.05
crystal system	monoclinic	orthorhombic
space group	P2 ₁ /n	P2 ₁ 2 ₁ 2 ₁
a, Å	13.096(3)	12.275(4)
b, Å	17.933(4)	14.171(9)
c, Å	15.994(3)	19.780(3)
β , deg	113.49(3)	
V, Å ³	3444.9(13)	3441(2)
Z	4	4
D _{calcd} , g cm ⁻³	1.525	1.587
$\lambda(\text{Mo K}\alpha)$, Å	0.710 73	0.710 73
μ , mm ⁻¹	1.155	1.213
R ^a	10.35	3.76
R _w ^b	9.65	4.20
T, K	293	293

$$^a R = \sum(|F_o| - |F_c|) / \sum|F_o|, \quad ^b R_w = [\sum w(|F_o| - |F_c|)^2 / \sum w|F_o|^2]^{1/2}.$$

absorption correction¹² was carried out. The scattering factors¹³ for neutral non-hydrogen atoms were corrected for both the real and the imaginary components of anomalous dispersion. The structures were determined by Patterson and Fourier methods for **1** and direct methods for **2** (SHELXTL PLUS). The structures were refined by a full-matrix least-squares technique; the function minimized was $\sum w(|F_o| - |F_c|)^2$ where $1/w = \sigma^2(F) + 0.003F^2$ for the Cu^{II}Cr^{III} (**1**) and $1/w = \sigma^2(F) + 0.0008F^2$ for the Cu^{II}Mn^{III} (**2**) compound. Idealized positions of H atoms bound to carbon atoms were calculated (C—H = 0.96 Å) and included in the refinement cycle.

A large number of dark red needles of the Cu^{II}Cr^{III} complex, **1**, had to be examined before a rather suitable specimen of the size $0.24 \times 0.24 \times 0.14$ mm³ could be selected, though it still suffered from poor diffraction quality and power. Cr, Cu, Cl, and O atoms were refined anisotropically for **1**. Perchlorate oxygen atoms of **1** showed large displacement parameters, indicating partial disorder of the perchlorate ions, which could not be resolved. Refinement converged at $R_w = 9.65\%$.

The diffraction intensities of an approximately $0.58 \times 0.20 \times 0.25$ mm³ black prism crystal of **2** were collected. All non-hydrogen atoms for the Cu^{II}Mn^{III} compound, **2**, were refined anisotropically. The carbon atom C(20), being statistically disordered over two sites, was refined with site occupancy factor 0.5 (split model). Refinement converged at $R_w = 4.20\%$. Final positional parameters are presented in Tables 2 and 3, while selected interatomic distances and angles are given in Tables 4 and 5 for the Cu^{II}Cr^{III} and Cu^{II}Mn^{III} compounds, respectively.

Results and Discussion

Synthesis. The monomeric [Cu(DopnH)(OH₂)]ClO₄ dissolves in methanol or water in the presence of a base with the concomitant formation of a neutral species [Cu(Dopn)(OH₂)]⁰, at least in part, as is evident from the formation of the dinuclear complexes containing the Cu(Dopn) unit. The function of added base is to provide a medium needed for the deprotonation of the O···H···O groups present in the solid [Cu(DopnH)(OH₂)]⁺, with the copper ions present in square pyramidal environments. The presumably square pyramidal neutral species [Cu(Dopn)(OH₂)]⁰ produced in this way can now function as a ligand for the coordinatively unsaturated ML³⁺ or 2⁺ units. In the presence of a counterion, e.g. ClO₄⁻, dark crystals are assembled in this manner in good yields (60–80%). The same type of reaction in the presence of acetate ions affords complexes containing a μ_2 -bridging acetate ion.

Infrared Spectra. The presence or absence of certain bands in the generally complicated IR spectra has been utilized to establish the nature of the complexes. Relevant bands are listed in Table 6. All of the perchlorate salts show strong bands near 1090–

(12) SHELXTL-PLUS program package (PC version) by G. M. Sheldrick, Universität Göttingen.

(13) *International Tables for X-ray Crystallography*; Kynoch: Birmingham, England, 1974; Vol. 4.

Table 2. Atomic Coordinates ($\times 10^4$) and Equivalent Isotropic Displacement Coefficients ($\text{\AA}^2 \times 10^3$) for 1

	x	y	z	U(eq) ^a
Cu	5567	2928	7100	68(3)
Cr	5627(4)	2637(3)	9508(3)	38(3)
Cl(1)	11533(17)	357(14)	8397(12)	98(10)
Cl(2)	10474(18)	6399(11)	11998(12)	106(10)
N(1)	3989(19)	3018(15)	9274(15)	29(7)
N(2)	6057(25)	3271(18)	10755(20)	63(10)
N(3)	5158(23)	1816(18)	10283(19)	57(10)
N(4)	5210(26)	2104(21)	7654(22)	77(11)
N(5)	5978(22)	3581(19)	8112(18)	50(9)
N(6)	6163(28)	3759(21)	6617(24)	80(12)
N(7)	5606(24)	2152(22)	6229(21)	67(11)
O(1)	4957(19)	2001(14)	8422(15)	62(8)
O(2)	5931(17)	3525(14)	8978(15)	56(7)
O(3)	3743(17)	3259(13)	6342(14)	46(7)
O(4)	7100(17)	2266(13)	9903(14)	52(7)
C(1)	4073(28)	3598(22)	9997(23)	63(12)
C(2)	5193(28)	3871(21)	10468(24)	51(12)
C(3)	5962(27)	2744(21)	11463(22)	49(10)
C(4)	5960(28)	1980(20)	11222(22)	48(11)
C(5)	3936(27)	1897(22)	10058(24)	56(12)
C(6)	3327(30)	2384(23)	9291(25)	67(12)
C(7)	3399(30)	3386(24)	8369(23)	69(13)
C(8)	7161(33)	3569(26)	10992(26)	93(15)
C(9)	5408(38)	1091(24)	10049(32)	104(17)
C(10)	5092(30)	1452(28)	7271(26)	58(12)
C(11)	4724(40)	735(27)	7502(32)	121(18)
C(12)	5356(33)	1514(30)	6405(28)	77(15)
C(13)	5173(53)	775(38)	5810(35)	217(32)
C(14)	6470(34)	4329(28)	7078(30)	75(14)
C(15)	6943(42)	5056(28)	6956(30)	110(18)
C(16)	6371(29)	4220(26)	8026(25)	54(12)
C(17)	6866(44)	4860(31)	8726(33)	129(20)
C(18)	5945(45)	2291(32)	5458(36)	137(21)
C(19)	6072(46)	3693(33)	5608(36)	153(23)
C(20)	6162(49)	2924(36)	5411(41)	161(26)
C(21)	7615(41)	2214(29)	9324(33)	134(20)
O(10)	11612(54)	-10(28)	9077(34)	259(48)
O(11)	11053(80)	932(44)	8229(50)	314(66)
O(12)	11018(77)	21(35)	7615(43)	303(59)
O(13)	12437(47)	431(44)	8421(55)	267(62)
O(20)	10773(98)	7060(33)	11989(61)	361(120)
O(21)	10916(34)	6003(27)	11528(19)	189(29)
O(22)	9390(34)	6426(41)	11620(28)	312(44)
O(23)	10809(29)	6142(22)	12873(23)	137(24)
O(w)	8781(31)	1634(22)	7165(25)	164(15)

^a Equivalent isotropic U defined as one-third of the trace of the orthogonalized U_{ij} tensor.

1100 cm^{-1} (antisymmetric stretch) and sharp bands at 620–625 cm^{-1} (antisymmetric bend), indicative of uncoordinated perchlorate anions.

Since the spectra of all complexes 1–9 are quite similar, the discussion is confined to the most important vibrations of the 4000–400 cm^{-1} region in relation to the structure. The monomeric $[\text{Cu}(\text{DopnH})(\text{OH}_2)]\text{ClO}_4 \cdot \text{H}_2\text{O}$ has appreciable IR absorption in the region of 2300 cm^{-1} due to the OH stretching vibrations of the hydrogen-bonded OHO group. These absorptions are missing in the spectra of the dinuclear complexes, indicating that the enolic hydrogen atoms are lost on chelation.

The medium-strong bands at 1192–1245 cm^{-1} are assignable¹⁴ to the NO stretching vibration. The second NO infrared absorption could not be observed for every dinuclear complex because of the occasional superposition of the bands originating from the perchlorate anions. However, for the hexafluorophosphate salt of the cation in complex 2a, the second NO stretch was identified unambiguously at 1116 cm^{-1} .

The $\nu(\text{CN})$ vibration is assigned to the band in the wavenumber regions 1633–1622 cm^{-1} for the imine and 1489–1558 cm^{-1} for

Table 3. Atomic Coordinates ($\times 10^4$) and Equivalent Isotropic Displacement Coefficients ($\text{\AA}^2 \times 10^3$) for 2

	x	y	z	U(eq) ^a
Cu	-285	5506	9858	42(1)
Mn	2145(1)	4344(1)	9373(1)	34(1)
N(1)	3880(5)	4797(4)	9592(3)	49(2)
N(2)	2851(6)	3011(4)	9605(3)	44(2)
N(3)	2819(5)	4065(4)	8416(3)	47(2)
N(4)	799(4)	5955(4)	9177(3)	38(2)
N(5)	729(5)	4781(4)	10448(3)	42(2)
N(6)	-1196(5)	5413(5)	10668(3)	54(2)
N(7)	-1117(5)	6547(5)	9427(4)	49(2)
O(1)	1837(3)	5615(3)	9103(2)	43(2)
O(2)	1756(4)	4479(4)	10299(2)	46(2)
O(3)	-961(4)	4406(4)	9224(2)	49(2)
O(4)	665(4)	3747(4)	9066(3)	51(2)
C(1)	4521(7)	3984(6)	9825(5)	65(3)
C(2)	3765(7)	3228(6)	10067(5)	63(3)
C(3)	3239(8)	2558(5)	8964(4)	64(3)
C(4)	2761(8)	3005(5)	8358(4)	63(3)
C(5)	3955(6)	4442(8)	8372(4)	68(3)
C(6)	4240(7)	5120(6)	8903(5)	69(3)
C(7)	3919(8)	5603(6)	10090(5)	74(4)
C(8)	2052(8)	2365(5)	9947(5)	56(3)
C(9)	2141(7)	4477(7)	7859(3)	58(3)
C(10)	512(6)	6665(5)	8809(4)	38(2)
C(11)	1224(7)	7115(5)	8302(4)	54(3)
C(12)	-625(6)	6954(5)	8930(4)	45(3)
C(13)	-1107(8)	7672(6)	8465(6)	71(4)
C(14)	-744(7)	5008(5)	11172(4)	51(3)
C(15)	-1246(9)	4892(7)	11865(4)	75(4)
C(16)	391(7)	4641(5)	11058(3)	46(3)
C(17)	1064(9)	4146(7)	11563(4)	76(4)
C(18)	-2281(7)	6777(7)	9609(6)	75(4)
C(19)	-2291(8)	5831(8)	10707(6)	87(4)
C(20a)	-2477(18)	6741(19)	10275(10)	79(9)
C(20b)	-2737(12)	5992(14)	10102(11)	59(7)
C(21)	-325(7)	3842(5)	8932(4)	41(3)
C(22)	-777(7)	3217(6)	8375(5)	58(3)
Cl(1)	5288(2)	7590(1)	8385(1)	61(1)
O(5)	5810(7)	8430(5)	8214(4)	105(3)
O(6)	5211(7)	7516(5)	9090(4)	103(3)
O(7)	4228(7)	7580(7)	8119(5)	135(4)
O(8)	5894(7)	6827(5)	8129(4)	102(3)
Cl(2)	396(2)	10509(2)	8130(1)	59(1)
O(9)	-715(5)	10718(6)	8249(4)	104(3)
O(10)	613(7)	9565(4)	8225(4)	115(3)
O(11)	1022(7)	11056(5)	8575(5)	127(4)
O(12)	646(8)	10691(8)	7461(4)	163(5)
O(1w)	7135(8)	4884(7)	8503(5)	133(4)
O(2w)	6200(7)	3142(6)	8311(5)	113(4)

^a Equivalent isotropic U defined as one-third of the trace of the orthogonalized U_{ij} tensor.

the oxime groups. The $\nu(\text{CN})$ vibration of the oximes for the dinuclear complexes containing trivalent metal ions is situated at a frequency significantly higher than that for the complexes containing the corresponding divalent metal ions, where these vibrations are found at 1490 cm^{-1} for Mn(II) and 1515 cm^{-1} for Co(II). This is in accord with the concept that on binuclear complex formation the positively charged ML^{3+} unit stabilizes the negative charge on oxygen of the oximate function¹⁵ and thus increases the double-bond character of the CN bond, which is expressed as a rise in the frequency. The strong bands in the wavenumber regions 1578–1571 and 1428–1410 cm^{-1} for 2, 2a, 3, 4a, 5a, and 7a are indicative of bridging acetato groups ($\Delta\nu(\text{CO}) = 168\text{--}143 \text{ cm}^{-1}$).

Electronic Spectra. Substantial energetic and distributional changes in the π -electron cloud of the $\text{C}=\text{N}$ group are observed on complex formation by the oxime ligand H_2Dopn , as is evidenced from IR spectroscopy. These changes should also be, in principle, observable in the optical spectra for the dinuclear complexes. Hence the optical spectra of the dinuclear complexes, together

(14) (a) Blinc, R.; Hadzi, D. *J. Chem. Soc. A* 1958, 4536. (b) Burger, K.; Ruff, I.; Ruff, F. *J. Inorg. Nucl. Chem.* 1965, 27, 179. (c) Caton, J. E.; Banks, C. V. *Inorg. Chem.* 1967, 6, 1670.

(15) Chakravorty, A. *Coord. Chem. Rev.* 1974, 13, 1.

Table 4. Selected Bond Lengths (Å) and Angles (deg) for [(Dopn)Cu(OH₂)Cr(OCH₃)L](ClO₄)₂·H₂O (**1**) (Esd's in Parentheses)

Cu—N(4)	1.876(39)	Cu—N(5)	1.893(30)
Cu—N(6)	1.977(41)	Cu—N(7)	1.984(37)
Cu—O(3)	2.285(19)	Cr—N(1)	2.173(26)
Cr—N(2)	2.166(31)	Cr—N(3)	2.165(35)
Cr—O(1)	1.968(23)	Cr—O(2)	1.920(27)
Cr—O(4)	1.895(22)		
N(4)—O(1)	1.406(49)	N(4)—C(10)	1.301(61)
N(5)—O(2)	1.414(41)	N(5)—C(16)	1.286(56)
N(6)—C(14)	1.230(60)		
N(7)—C(12)	1.252(66)		
N(4)—Cu—N(5)	97.1(15)	N(4)—Cu—N(6)	172.0(13)
N(5)—Cu—N(6)	81.2(15)	N(4)—Cu—N(7)	81.9(16)
N(5)—Cu—N(7)	162.9(11)	N(6)—Cu—N(7)	97.5(16)
N(4)—Cu—O(3)	92.9(11)	N(5)—Cu—O(3)	100.0(10)
N(6)—Cu—O(3)	95.1(11)	N(7)—Cu—O(3)	97.1(10)
N(1)—Cr—N(2)	82.4(11)	N(1)—Cr—N(3)	79.8(11)
N(2)—Cr—N(3)	81.9(12)	N(1)—Cr—O(1)	88.1(10)
N(2)—Cr—O(1)	167.9(13)	N(3)—Cr—O(1)	89.1(11)
N(1)—Cr—O(2)	91.6(10)	N(2)—Cr—O(2)	87.0(12)
N(3)—Cr—O(2)	166.7(13)	O(1)—Cr—O(2)	100.9(10)
N(1)—Cr—O(4)	171.1(10)	N(2)—Cr—O(4)	91.2(11)
N(3)—Cr—O(4)	93.1(11)	O(1)—Cr—O(4)	97.3(10)
O(2)—Cr—O(4)	94.3(10)		

Table 5. Selected Bond Lengths (Å) and Angles (deg) for [(Dopn)Cu(μ-OOCCH₃)MnL](ClO₄)₂·H₂O (**2**) (Esd's in Parentheses)

Cu—N(4)	1.996(6)	Cu—N(5)	1.992(6)
Cu—N(6)	1.958(7)	Cu—N(7)	1.986(7)
Cu—O(3)	2.166(5)	Mn—N(1)	2.266(6)
Mn—N(2)	2.128(6)	Mn—N(3)	2.104(6)
Mn—O(1)	1.916(5)	Mn—O(2)	1.902(5)
Mn—O(4)	2.093(6)		
N(4)—O(1)	1.371(7)	N(4)—C(10)	1.291(9)
N(5)—O(2)	1.363(8)	N(5)—C(16)	1.291(9)
		N(6)—C(14)	1.277(11)
		N(7)—C(12)	1.290(11)
N(4)—Cu—N(5)	98.2(2)	N(4)—Cu—N(6)	162.5(3)
N(5)—Cu—N(6)	81.0(3)	N(4)—Cu—N(7)	79.0(2)
N(5)—Cu—N(7)	162.9(3)	N(6)—Cu—N(7)	96.2(3)
N(4)—Cu—O(3)	95.4(2)	N(5)—Cu—O(3)	102.0(2)
N(6)—Cu—O(3)	101.9(2)	N(7)—Cu—O(3)	95.1(2)
N(1)—Mn—N(2)	80.1(2)	N(1)—Mn—N(3)	81.7(2)
N(2)—Mn—N(3)	82.2(2)	N(1)—Mn—O(1)	88.4(2)
N(2)—Mn—O(1)	167.0(2)	N(3)—Mn—O(1)	90.1(2)
N(1)—Mn—O(2)	91.4(2)	N(2)—Mn—O(2)	89.1(2)
N(3)—Mn—O(2)	169.8(2)	O(1)—Mn—O(2)	97.2(2)
N(1)—Mn—O(4)	170.1(2)	N(2)—Mn—O(4)	93.3(2)
N(3)—Mn—O(4)	90.2(2)	O(1)—Mn—O(4)	97.3(2)
O(2)—Mn—O(4)	95.9(2)		

with the monomeric [Cu(DopnH)(OH₂)]ClO₄, the free oxime H₂Dopn, and its deprotonated form Dopn²⁻ in basic medium, have been measured in methanol in the range 200–1200 nm. The absorption maxima with the corresponding extinction coefficients are given in Table 7. The spectra of the complexes are dominated by charge-transfer transitions in the UV–vis regions.

The absorption maximum of the free ligand H₂Dopn at 227 nm is due to π–π* transitions of the C=N group and shifts, as is expected, to lower energy at 276 nm in basic medium due to deprotonation of the OH groups. For the mononuclear [Cu(DopnH)(OH₂)]⁺, apart from the ligand band at 237 nm, there are absorptions at 274 and 300 nm. Metal to ligand charge-transfer (MLCT) transitions can occur in complexes where the unsaturated ligands like oximes, which contain empty antibonding π orbitals, are bonded to oxidizable metals. Judged on the basis of high extinction coefficients, the last mentioned two bands are ascribed to these charge-transfer transitions. The transition is thought to be the (yz ± izx)–π*_{oxime} in character. Medium-strong bands are found at 486 nm for Cu(DopnH)⁺ and 535 nm

for Cu(Dopn)⁰ (Cu(DopnH)⁺ in basic medium) on the low-energy side of the charge-transfer bands. This transition is considered to be a spin-allowed d–d transition, as has been described previously in the literature.¹⁶

In the wavelength range 200–365 nm, the spectra of the dinuclear complexes disclose character nearly identical with that of the Cu(Dopn)⁰ unit, indicating that the energy states of π-electron system of the Dopn²⁻ anion suffer no substantial alterations on complex formation. However, the extinction coefficients measured at nearly identical wavelengths show significant differences. The dinuclear complexes in general exhibit three bands in the region 200–365 nm due to the intraligand π–π* and MLCT transitions with very high extinction coefficients. These complexes are dark brown to practically black and owe their origin of color to these CT transitions. The symmetry-forbidden d–d bands are in many cases obscured by the more intense bands due to symmetry-allowed CT transitions.

Interestingly, we have not observed any d–d band for **1** that could be unambiguously assigned to the Cr(III) center. Complex **2** exhibits a very broad intense band at 560–575 nm. Probably this band, d–d in nature, originates from both the Cu(II) and the ⁵T_{2g} ← ⁵E_g transitions at the Mn(III) center. The sharp band at 412 nm for **3** can be assigned to the Mn(II) center due to the ⁴A_{1g}(G), ⁴E_g(G) ← ⁶A_{1g} transitions,¹⁷ although this predicted forbidden transition should be weak in intensity. This formally forbidden band for the Mn(II) chromophore is activated by an exchange mechanism, as might be the shoulder at ~490 nm for **4**. Complex **5** exhibits several d–d bands in the range 425–1010 nm due to the transitions at Cu(II) and Co(II) centers. However, the weak band at 1010 nm can be unambiguously assigned to the ⁴T_{2g} ← ⁴T_{1g} transition of the Co(II) center. The Cu(II) bands for **7** are difficult to recognize. On the other hand, the bands at 787 and 1015 nm definitely originate from the Ni(II) center due to ³T_{1g}(F) ← ³A_{2g} and ³T_{2g} ← ³A_{2g} transitions. The band at 928 nm of complex **8** originates from the Cu(C₉H₂₁N₃) unit. This assignment is in complete accord with our earlier observations in Cu(II) chemistry with this macrocyclic amine.¹⁸

The Cu^{II}Zn^{II} complex, **9**, exhibits a single d–d band at 520 nm due to the presence of d⁹ Cu(II). On the basis of this and our earlier observations in Cu(II) chemistry with the oxime ligands,¹⁹ we assign the shoulders and peaks in the range 500–590 nm to the spin-allowed d–d transitions occurring mostly at the Cu(Dopn) unit, strongly indicating the presence of five-coordinate copper(II) ions. The extinction coefficients are in some cases large, in spite of the Laporte g → g selection rule, because of the extensive mixing of the metal d orbitals with the ligand orbitals and because of their proximity to other CT bands.

It has been shown by Hathaway²⁰ that it is possible to predict the stereochemistry of the local copper(II) environment in Cu(II) complexes of unknown crystal structure from the positions and intensities of d–d transitions of CuX₅ chromophores. In general, trigonal bipyramidal complexes with ²A₁ ground states exhibit a single relatively intense band at 12 500 ± 1500 cm⁻¹; on the other hand, the electronic spectra of square based pyramidal complexes consist of two clearly resolved bands covering the range (1500 ± 2000) cm⁻¹. On the basis of the above knowledge, a pseudo square pyramidal geometry is assigned to Cu(II) centers in all complexes synthesized (Table 7) rather than a trigonal bipyramidal geometry. The electronic spectral results indicate

(16) Nishida, Y.; Hayashida, K.; Sumita, A.; Kida, S. *Inorg. Chim. Acta* **1978**, *31*, 19.

(17) Lever, A. B. P. *Inorganic Electronic Spectroscopy*; Elsevier: Amsterdam, 1984.

(18) Chaudhuri, P.; Oder, K. *J. Chem. Soc., Dalton Trans.* **1990**, 1597.

(19) Chaudhuri, P.; Winter, M.; Della Védova, B. P. C.; Bill, E.; Trautwein, A. X.; Gehring, S.; Fleischhauer, P.; Nuber, B.; Weiss, J. *Inorg. Chem.* **1991**, *30*, 2148.

(20) (a) Hathaway, B. J.; Tomlinson, A. A. G. *Coord. Chem. Rev.* **1970**, *5*, 1. (b) Hathaway, B. J.; Billing, D. E. *Coord. Chem. Rev.* **1970**, *5*, 143. (c) Hathaway, B. J. *Struct. Bonding (Berlin)* **1984**, *57*, 55.

Table 6. Selected IR Spectral Data^a

complex	ν , cm ⁻¹
[(Dopn)Cu ^{II} (OH ₂)Cr ^{III} (OCH ₃)L](ClO ₄) ₂ ·H ₂ O (1)	ν (OH) 3518 m (sh) ν (CN) 1633 m (sh), 1536 m (sh)
[(Dopn)Cu ^{II} (μ -OOCCH ₃)Mn ^{III} L](ClO ₄) ₂ ·2H ₂ O (2)	ν (NO) 1219 m (sh), 1145 s (sh) ν (OH) 3640, 3430 s (sh) ν (CN) 1632 m (sh), 1588 s (sh) ν (NO) 1233 m (sh)
[(Dopn)Cu ^{II} (μ -OOCCH ₃)Mn ^{III} L](PF ₆) ₂ ·2H ₂ O (2a)	ν (COO) 1572 s (sh), 1419 s (sh) ν (OH) 3647 m (sh), 3436 s (br) ν (CN) 1633 m (sh) ν (NO) 1192 m (sh), 1116 w (sh) ν (COO) 1571 s (sh), 1428 m (sh)
[(Dopn)Cu ^{II} (μ -OOCCH ₃)Mn ^{II} L](ClO ₄) (3)	ν (CN) 1612 m (sh), 1490 s (sh) ν (NO) 1234 s (sh), 1147 s (sh)
[(Dopn)Cu ^{II} (OH ₂)Fe ^{III} (Cl)L](ClO ₄) ₂ (4)	ν (COO) 1572 s (sh), 1413 s (sh) ν (OH) 3620 m (sh), 3515 m (sh) ν (CN) 1633 m (sh), 1538 m (sh)
[(Dopn)Cu ^{II} (μ -OOCCH ₃)Fe ^{III} L](ClO ₄) ₂ ·H ₂ O (4a)	ν (NO) 1216 m (sh), 1150 s (sh) ν (OH) 3640, 3436 m (sh) ν (CN) 1631 m (sh) ν (NO) 1150 (sh)
[(Dopn)Cu ^{II} (OH ₂)Co ^{III} (Cl)L](ClO ₄) (5)	ν (COO) 1571, 1410 s (sh) ν (OH) 3582, 3502 m (sh) ν (CN) 1613 m (sh), 1515 s (sh)
[(Dopn)Cu ^{II} (μ -OOCCH ₃)Co ^{II} L](ClO ₄) (5a)	ν (NO) 1233, 1150 s (sh) ν (CN) 1618 (sh), 1495 m (sh)
[(Dopn)Cu ^{II} (OH ₂)Co ^{III} (Cl)L](ClO ₄) ₂ (6)	ν (NO) 1236, 1147 s (sh) ν (COO) 1578, 1411 s (sh)
[(Dopn)Cu ^{II} (OH ₂)Ni ^{III} (OH ₂)L](ClO ₄) ₂ ·H ₂ O (7)	ν (OH) 3637 m (sh), 3430 m (br) ν (CN) 1613 m (sh), 1538 s (sh) ν (NO) 1220 m (sh)
[(Dopn)Cu ^{II} (μ -OOCCH ₃)Ni ^{II} L](ClO ₄) (7a)	ν (OH) 3490 s(br) ν (CN) 1620 m (sh), 1500 s (sh) ν (NO) 1240 m (sh), 1156 s (sh) ν (CN) 1618 m (sh), 1489 s (sh) ν (NO) 1245, 1152 vs (sh)
[(Dopn)Cu ^{II} (OH ₂)Cu ^{II} L](ClO ₄) ₂ ·2H ₂ O (8)	ν (COO) 1577 vs (sh), 1411 s (sh) ν (OH) 3576, 3540 m (sh) ν (CN) 1625 m (sh), 1521 s (sh)
[(Dopn)Cu ^{II} (OH ₂)Zn ^{II} (OH ₂)L](ClO ₄) ₂ ·H ₂ O (9)	ν (NO) 1226 m (sh), 1147 s (sh) ν (OH) 3590 s (sh), 3436 s (br) ν (CN) 1622 m (sh), 1510 s (sh) ν (NO) 1237 s (sh), 1151 vs (sh)

^a Key: vs = very strong; s = strong; m = medium; w = weak; sh = sharp; br = broad.

Table 7. Electronic Spectral Data for the Dinuclear Complexes in Methanol at Ambient Temperature

complex	λ_{max} , nm (ϵ , L mol ⁻¹ cm ⁻¹)
Cu ^{II} Cr ^{III} (OCH ₃) (1)	220 sh (17 500), 236 (18 740), 278 (13 040), ~530 sh (350)
Cu ^{II} Mn ^{III} (OAc) (2)	245 (18 320), 280 sh (14 100), 311 (13 820), 560–575 br (1020)
Cu ^{II} Mn ^{II} (OAc) (3)	253 (14 710), 275 sh (12 400), 320 (10 450), 412 (923), 450 sh (600), 540 (603), 585 sh (570)
Cu ^{II} Fe ^{III} (Cl) (4)	245 (20 640), ~270 sh (15 500), 345 sh (7340), 490 sh (380), 565 sh (220), 1250 (4)
Cu ^{II} Co ^{III} (Cl) (6)	240 (23 950), 299 (18 180), 365 sh (5300), 505–520 sh (506)
Cu ^{II} Co ^{II} (Cl) (5)	250 (15 270), 308 (12 220), 425 sh (1000), 540 sh (440), 585 sh (360), 673 (199), 1010 (9.8)
Cu ^{II} Ni ^{III} (OH ₂) (7)	250 (15 470), 275 sh (11 700), 319 (11 210), 787 (31), 1015 (19)
Cu ^{II} Cu ^{II} (8)	249 (16 990), 300 sh (11 300), 325 (13 490), 435 (2470), 575 sh (630), 928 (24)
Cu ^{II} Zn ^{II} (OH ₂) (9)	247 (16 780), 275 sh (11 000), 314 (12 540), 520 (233)
[Cu(dopnH)] ⁺	237 (13 880), 274 (7720), 300 sh (6400), 486 (205)
[Cu(dopn)] ⁰	251 (12 520), 282 (12 420), 310 sh (9400), 535 (400)
dopnH ₂	227 (17 100)
dopn ²⁻	276 (>13 000)

that the complexes 1–9 are stable and retain their discrete dinuclear entity also in solution.

Molecular Structure of [(Dopn)Cu^{II}(OH₂)Cr^{III}(OCH₃)L](ClO₄)₂·H₂O (1). The complex molecule consists of a dicationic dinuclear unit, two disordered perchlorate anions, and a water molecule. The cation together with the atom-labeling scheme is used in Figure 1. Selected bond lengths and angles are listed in Table 4. The copper ion is in a distorted square pyramidal environment with four nitrogens in the basal plane and the fifth, apical, position occupied by a water molecule. Each five-membered chelate ring containing Cu includes an oxime nitrogen and an imine nitrogen; the six-membered chelate ring includes two imine nitrogens. The Cu—N bond lengths fall in the range

1.876–1.977 Å and are considered as normal covalent bonds. The axial Cu—O(3) bond is longer, 2.285(19) Å, as is expected for square pyramidal complexes of copper(II) and has been observed earlier.¹⁹ The copper ion is 0.21 Å out of the best basal plane comprising the four nitrogen atoms N(4)N(5)N(6)N(7) in the direction of the coordinated water oxygen O(3). Thus the metrical parameters for the Cu center in **1** are similar in magnitude to those reported in the literature for the [Cu(DopnH)(OH₂)]⁺ complex cation.²¹

(21) (a) Bertrand, J. A.; Smith, J. H.; van Derveer, D. G. *Inorg. Chem.* **1977**, *6*, 1484. (b) Anderson, O. P.; Packard, A. B. *Inorg. Chem.* **1979**, *7*, 1940.

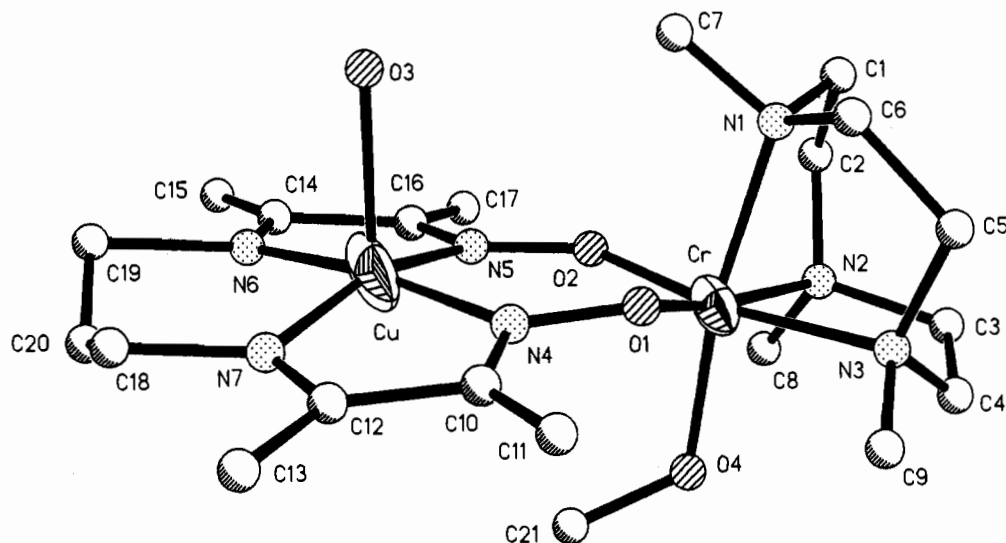


Figure 1. Molecular structure of the dinuclear $\text{Cu}^{\text{II}}\text{Cr}^{\text{III}}$ cation in **1**, showing the atom-numbering scheme.

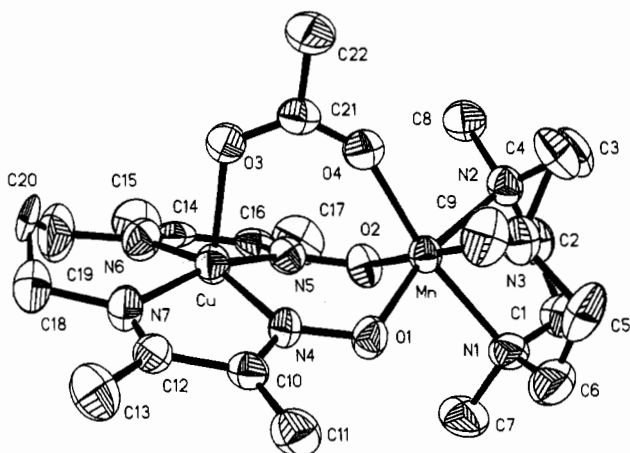


Figure 2. ORTEP view of the dinuclear $\text{Cu}^{\text{II}}\text{Mn}^{\text{III}}$ cation in **2**.

The chromium coordination geometry is distorted octahedral with three nitrogen atoms from the facially coordinated tridentate macrocyclic amine and three oxygen atoms, O(1) and O(2) from the bridging oximate group and the third from a monodentate methoxy group, O(4). The Cr—N (average 2.16(2) Å) and Cr—O (average 1.92(2) Å) distances correspond to the literature values for Cr(III) complexes with this macrocyclic amine.⁷ A deviation from idealized orthogonal geometry is found for the ligand L, the N—Cr—N angles ranging between 79.8(11) and 82.4(11)°, whereas O—Cr—O angles fall between 94.3(10) and 100.9(10)°. The chromium ion is displaced by 0.15 Å from the mean basal N(2)N(3)O(1)O(2) atoms toward the apical oxygen atom O(4) of the methoxy group.

The binuclear skeleton is not coplanar but is slightly bent with a Cu···Cr separation of 3.86 Å. The dihedral angle between the planes CuN(4)N(5)N(6)N(7) and CrN(2)N(3)O(1)O(2) is 14°. It is interesting to note that the coordinated water, O(3), at the Cu center is situated at an antiposition with respect to the methoxy group, O(4), of the Cr(III) center. Thus the structure can be described as resulting from the sharing of an edge between a square pyramid and an octahedron.

The ligand L exhibits no unexpected features. Comparatively short C—C bond lengths (average 1.44(2) Å) between the methylene groups of the macrocyclic amine ligand L may be attributed to the effects of libration.

Molecular Structure of [(Dopn)Cu^{II}(μ-CH₃COO)Mn^{III}L]₂(ClO₄)₂·2H₂O (2**).** Figure 2 shows a perspective view of the cation in **2** with the atom-labeling scheme in the asymmetric unit. Selected bond distances and angles are listed in Table 5. The

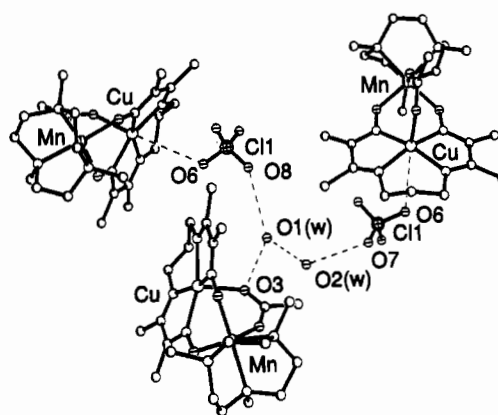


Figure 3. Intermolecular hydrogen-bonding network in **2**.

structural data concerning the ligand parts of the complex are in good agreement with the previous studies dealing with compounds of the same ligands and do not warrant any additional comment. The ring conformation of the macrocyclic amine ligand L in the complex **2** is $\delta\delta\delta$. The structure of the complex molecule consists of a dicationic asymmetric unit, two well-separated perchlorate anions, and two molecules of water of crystallization. The X-ray structure confirms that a heterodinuclear complex with a Cu···Mn distance of 3.539 Å has indeed been formed as a result of the sharing, in a very broad sense, of a face between a square pyramid and an octahedron. The coordination environment around the copper atom is distorted square pyramidal with four nitrogens at the equatorial planes and the carboxylate oxygen O(3) of the bridging acetate group at the axial position, Cu—O(3) = 2.166(5) Å. The Cu—N bond lengths fall in the range 1.958(7)–1.992(6) Å, slightly elongated compared with the Cu—N bonds²¹ in [Cu(DopnH)]ClO₄ (1.937(5)–1.961(5) Å). The copper ion is displaced by 0.3 Å from the mean basal plane of the four nitrogen atoms, N(4)N(5)N(6)N(7), of the Dopn ligand toward the apical oxygen atom O(3).

One of the oxygen atoms of a perchlorate anion is situated at an axial position, trans to O(3), of the Cu ion with a separation of Cu···O(6) = 3.544 Å and can be considered as nonbonding. An intermolecular hydrogen-bonding network (Figure 3) is present between the oxygen atoms O(7) and O(8) of a perchlorate anion Cl(1), two molecules of water, O(1w) and O(2w), and the O(3) atom of the acetate group with the following bond separations: O(7)—O(2w) = 2.985, O(2w)—O(1w) = 2.748, O(1w)—O(3) = 2.820, O(1w)—O(8) = 3.233 Å. Hydrogen atoms of the water molecules could not be located, except one, H(2w), which was introduced in the refinement cycle.

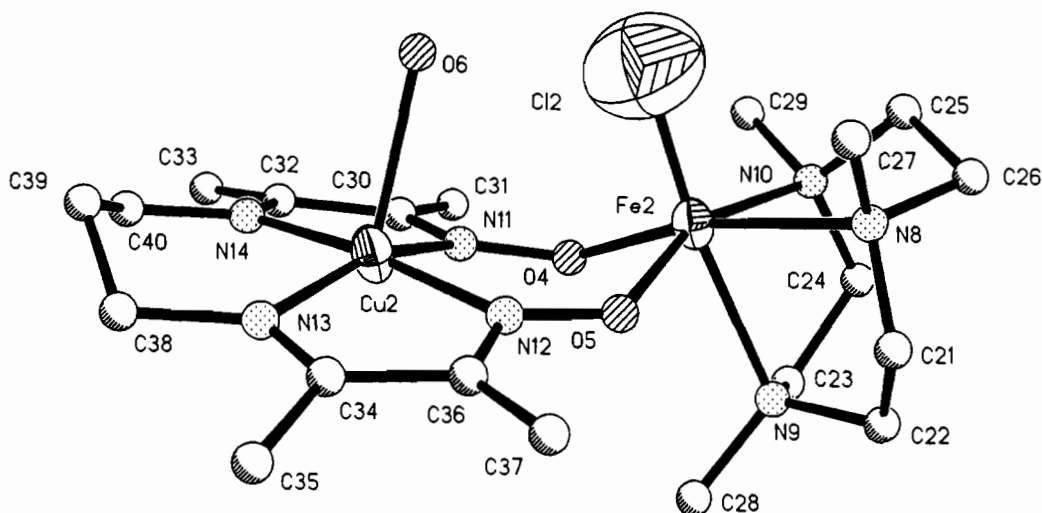


Figure 4. Structure of the dinuclear dication Cu^{II}Fe^{III} in 4.

The manganese coordination geometry is distorted octahedral with three nitrogen atoms from the facially coordinated tridentate macrocyclic amine and three oxygen atoms, two from the bridging oximate group and one from the bridging acetate group. The manganese ion is out of the plane comprising O(1)O(2)N(2)N(3) by 0.15 Å toward the oxygen atom O(4) of the acetate group. The largest deviation from idealized 90° interbond angles is 9.9°, which occurs within the five-membered C—C—N—Mn—N chelate rings, the N—Mn—N angles ranging between 80.1(2) and 82.3(2)°, whereas the O—Mn—O angles fall between 95.9(2) and 97.3(2)°. O(1), O(2), N(2), and N(3) from the basal plane of the tetragonally distorted octahedron for the manganese ion with Mn—O(av) = 1.909(7) Å and Mn—N(av) = 2.116(12) Å. The axial Mn—O(4) and Mn—N(1) bond lengths, 2.093(6) and 2.266(6) Å, respectively, are substantially elongated as a consequence of the Jahn–Teller distortion of the Mn(III) ion. Thus the bond lengths are consistent with a d⁴ high-spin electron configuration of the Mn(III) center.

The binuclear cation is not coplanar but is bent with a dihedral angle between the planes CuN(4)N(5)N(6)N(7) and MnO(1)O(2)N(2)N(3) of 40.6°.

Structure of [(Dopn)Cu^{II}(OH₂)Fe^{III}(Cl)L](ClO₄)₂ (4).²² Although the analytical and spectroscopic data unambiguously showed the presence of a dinuclear CuFe core as the smallest unit in the cation, an X-ray analysis was undertaken to remove the doubts regarding connectivity. Unfortunately, crystals of the cation as its perchlorate salt diffract X-rays very weakly. In spite of the high *R* factor and large standard deviations due to the limited data of a weakly diffracting small crystal, the crystal structure analysis of 4 confirmed its heterobinuclear structure. Because of its unacceptable quality, we are refraining from publishing the crystal data in detail. The structure consists of distinct [(Dopn)Cu^{II}(OH₂)Fe^{III}(Cl)L]²⁺ cations and noncoordinatively bound perchlorate anions (Figure 4). The asymmetric unit cell contains two independent molecules. The iron center Fe(2) is 6-fold coordinated, the N(10), N(8) of the cyclic amine and O(4), O(5) of the oxime oxygens forming the equatorial plane of an octahedron, the apexes of which are occupied by a nitrogen N(9) of the ligand L and a chlorine atom Cl(2). The metrical parameters and coordination geometry of the Cu center are similar to those of the Cu center in 1. The Fe–N (average 2.21 Å) and Fe–O (average 1.94 Å) bond lengths are in accord with a d⁵ high-spin electron configuration of the Fe(III) center. In contrast to the structure of 1, the coordinated water molecule O(6) at the Cu center and the chloride ion Cl(2) at the Fe center

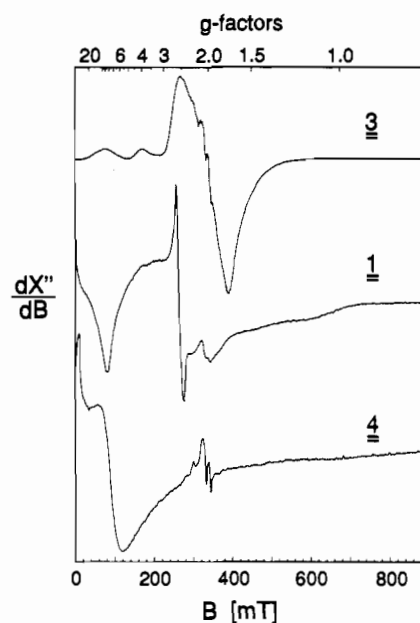


Figure 5. EPR spectra of methanolic solutions of complexes 1, 3, and 4 at 4.2 K. Experimental conditions: modulation amplitude 1 mT, modulation frequency 100 kHz, microwave power 20 μW, microwave frequency 9.433 GHz.

are in the cis positions. As is expected, the cation is bent with a dihedral angle of 23.2° between the CuN₄ and FeN₂O₂ planes. The nonbonded Cu···Fe separation is 3.66 Å. The iron ion is situated 0.29 Å above the basal plane toward the apical chlorine atom.

EPR Studies. X-band EPR spectra of complexes 1–9 were recorded both on powder samples and in methanolic solutions at low temperature (3.0–77 K) in order to establish the electronic ground state of the heterodinuclear complexes. Significant contributions from excited states were not observed in the measured temperature range, due to strong exchange splitting of spin states. This is consistent with magnetic susceptibility measurements, described below.

Solid 5a, Cu^{II}Co^{II}, with an apparently diamagnetic ground state is EPR silent under our experimental conditions. Interestingly, three other integer-spin systems (*S* = 2) of the series, Cu^{II}–Cr^{III} (1), Cu^{II}Mn^{II} (3), and Cu^{II}Fe^{III} (4), are EPR active, which reveals weak zero-field splitting within the *S* = 2 multiplets of these compounds. EPR spectra of methanol solutions of 1, 3, and 4 are depicted in Figure 5. Polycrystalline samples also yield integer-spin EPR spectra; however, due to intermolecular spin coupling in the solid state, they hardly resemble the solution spectra

(22) [C₂₀H₄₁N₇O₃ClCuFe](ClO₄)₂, monoclinic space group, *Pc*, *a* = 8.317(3) Å, *b* = 24.341(9) Å, *c* = 15.877(6) Å, β = 90.30(2)°, *V* = 3214.2 Å³, *Z* = 4, final *R* = 0.109 for 2884 unique observed intensities.

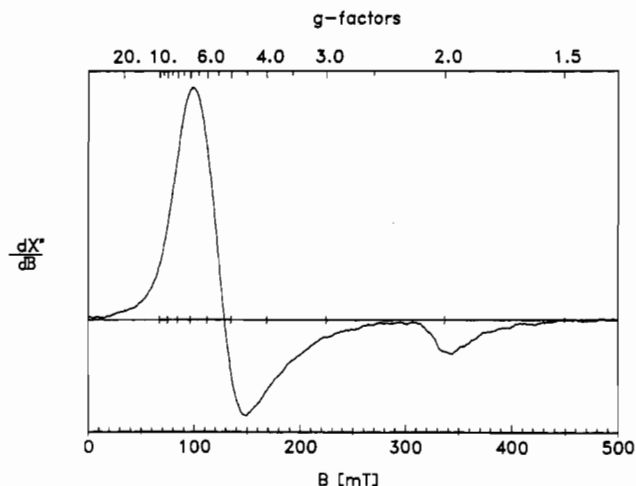


Figure 6. EPR spectrum of polycrystalline complex **2** at 77 K. Experimental conditions: modulation amplitude 1 mT, modulation frequency 100 kHz, microwave power 200 μ W, microwave frequency 9.430 GHz.

and, hence, were discarded. The resonances of the solution spectra are broad and extend over a wide field range from zero to more than 500 mT. (Weak narrow lines at $g \sim 2$ are due to $S = 1/2$ contaminations in the solution and will not be regarded.) The wide distribution of integer-spin signals indicates that, under experimental conditions of X-band EPR, zero-field interaction and Zeeman interaction are comparable and correspond to the energy of X-band resonances ($h\nu = 0.3 \text{ cm}^{-1}$). Under these conditions magnetic substates are severely mixed and level splittings depend strongly on field strength and field direction within the molecular frame. The EPR resonances, therefore, depend on the orientation of molecules in frozen solution and, hence, are spread over a wide range of applied fields. From such complex integer-spin EPR spectra, g tensors of the spin quintets cannot be derived without explicit simulations. The situation would be more transparent under the following conditions. EPR-active $S = 2$ systems with clearly dominating zero-field interaction ($D > h\nu$) would show the typical “ $g = 12$ ” pattern, as observed for cytochrome *c* oxidase and related Fe–Cu model complexes.²³ Those signals arise from pseudo-“ $\Delta m = 4$ ” transitions within distinct and energetically isolated “ $m_s = \pm 2$ ” sublevels. On the other hand, vanishing zero-field interaction ($D \ll h\nu$) essentially would lead to collapsed EPR spectra centered at $g \sim 2$.

The Mn(II) complex **3** appears to be closest to the limiting case of vanishing zero-field interaction. Its solution spectrum at 4.2 K is almost centered at $g = 2$ (Figure 5). The Cr(III) and Fe(III) complexes **1** and **4** exhibit spectral features with a prominent low-field trough, indicating stronger zero-field interaction in **1** and **4** compared to **3**.

The EPR patterns of **1**, **3**, and **4** are temperature-independent with a Curie–Weiss behavior of EPR amplitudes in the range 3–50 K. This result imposes constraints on the total splitting of the ground-state spin quintets to values less than 3 K and thus corroborates the above finding, i.e. weak zero-field interaction in **1**, **3**, and **4**.

Figure 6 shows the powder spectrum for **2** at 77 K. The spectrum displays wide signals at effective g values $g_{\perp} \sim 6$, $g_{\parallel} \sim 2$. Very similar features are observed from solution spectra in the temperature range 4.2–100 K. In solution, however, this pattern is obscured in the $g = 2$ region by superposition of preparation-dependent Mn(II) signals. The effective g values of **2** are typical for an energetically separate $|m_s = \pm 1/2\rangle$ Kramers

doublet of a spin sextet ($S = 5/2$) with quasi axial ligand-field symmetry and moderate strength of zero-field interaction ($D \geq \sim h\nu$). Thus, the EPR spectra corroborate the finding of ferromagnetic exchange coupling between Cu(II) ($S = 1/2$) and Mn(III) ($S = 2$) in complex **2**. The effective g_{\perp} values of the spectra of complex **2** are slightly below 6, the theoretical value for energetically well-separated Kramers doublets $|m_s = \pm 1/2\rangle$ (with the electronic g value of the spin quintet taken equal to 2). This situation indicates mixing of excited Kramers doublets $|m_s = \pm 1/2\rangle$ and, hence, demonstrates that the zero-field parameter D of complex **2** is very small. From our experience with other $S = 5/2$ systems, we propose that D does not exceed the value of 1 cm^{-1} .

Spin multiplets in the complexes under study here are well separated by exchange interaction (see below). Under this condition, the effective zero-field parameter and g values of the different spin multiplets of each complex can be related to local values of individual metal ions with spin-dependent weight factors derived from the Wigner–Eckart theorem.^{2,25} For the ground-state spin quintet of **2**, the corresponding expressions are $D_{5/2} = 3/5 D_{\text{Mn(III)}}$ and $g_{5/2} = 4/5 g_{\text{Mn(III)}} + 1/5 g_{\text{Cu}}$, respectively. With the crude estimate $D_{5/2} \leq \sim 1 \text{ cm}^{-1}$, taken from above, the relation for $D_{\text{Mn(III)}}$ yields $D_{\text{Mn(III)}} \leq \sim 2 \text{ cm}^{-1}$, which is fairly low for Mn(III). However, this value is consistent with a local g value $g_{\text{Mn(III)}}$ close to 2.0, as it can be estimated from the expression for $g_{\text{Mn(III)}}$, if one adopts $g_{5/2} = 2.0$, taken from the EPR spectrum (Figure 6), and $g_{\text{Cu}} = 2.1$, taken from the Cu^{II}Zn^{II} complex **9**, shown below.

Powder spectra of **6**, **7**, and **9**, recorded at 10 K, can be readily simulated by adopting spin $S = 1/2$ and quasi-isotropic g values (**6**, $g = 2.197, 2.067, 2.059$; **7**, $g = 2.236, 2.208, 2.159$; **9**, $g = 2.205, 2.054, 2.038$). This proves the ground state to be a spin doublet in those complexes. The relatively small line width and the lack of hyperfine splitting by the ^{59}Co ($I = 7/2$) nucleus are clear indications that **6** is a genuine Cu^{II}Co^{III} species with localized Cu^{II} ($S_{\text{Cu}} = 1/2$), Co^{III} ($S_{\text{Co}} = 0$) oxidation states. The average g values obtained from fits of EPR spectra are $g_{\text{av}} = 2.096$ and 2.101 for **6** and **9**, respectively, consistent with the presence of magnetic monomers, the spin of which originates only from Cu(II), $S_{\text{Cu}} = 1/2$. For the Ni complex **7**, the significantly higher value of $g_{\text{av}} = 2.201$ is related to antiparallel spin coupling of $S_{\text{Cu}} = 1/2$ and $S_{\text{Ni}} = 1$. The ground-state properties of **7** are dominated by Ni(II), according to the relation^{2,25} $g_{1/2} = -1/3 g_{\text{Cu}} + 4/3 g_{\text{Ni}}$. Taking as local values for Cu(II) $g_{\text{Cu}} \sim 2.10$, from **6** and **9**, the local value for Ni(II) becomes $g_{\text{Ni}} = 2.18$, which is in complete accord with g values reported for d⁸ Ni(II) with 6-fold coordination.

Complex **8** is EPR inactive at 10 K, suggesting that the exchange is antiferromagnetic with a diamagnetic ($S = 0$) ground state. The fact that no resonances are observed even at 50 K indicates that the $S = 1$ state of the Cu(II)–Cu(II) dimer is significantly higher in energy than the $S = 0$ state, supporting the result obtained from susceptibility measurements (see below).

Magnetic Susceptibility Studies. Magnetic susceptibility data for polycrystalline samples of complexes **1–9** were collected in the temperature range 2–295 K in order to characterize the sign and magnitude of the magnetic exchange interaction propagated by the oxime bridging ligand. The magnetic analysis was carried

(23) Juarez-Garcia, C.; Hendrick, M. P.; Holman, T. R.; Que, L.; Münck, E. *J. Am. Chem. Soc.* **1991**, *113*, 518.

(24) Luneau, D.; Oshio, H.; Okawa, H.; Koikawa, M.; Kida, S. *Bull. Chem. Soc. Jpn.* **1990**, *63*, 2212.

(25) (a) Chao, C. C. *J. Magn. Reson.* **1973**, *10*, 1. (b) Scaringe, R. P.; Hodgson, D. J.; Hatfield, W. E. *Mol. Phys.* **1978**, *35*, 701.

(26) (a) Kahn, O.; Tola, P.; Coudanne, H. *Chem. Phys.* **1979**, *42*, 355. (b) Torihara, N.; Okawa, H.; Kida, S. *Chem. Lett.* **1978**, *5*, 45.

(27) Andrew, J. E.; Ball, P. W.; Blake, A. B. *J. Chem. Soc., Chem. Commun.* **1969**, 143.

(28) Tola, P.; Kahn, O.; Chauvel, C.; Coudanne, H. *Now. J. Chim.* **1979**, *1*, 467.

(29) Lloret, F.; Ruiz, R.; Julve, M.; Faus, J.; Journaux, Y.; Castro, I.; Verdager, M. *Chem. Mater.* **1992**, *4*, 1150.

(30) Zhong, J. Z.; Okawa, H.; Matsumoto, N.; Sakiyama, H.; Kida, S. *J. Chem. Soc., Dalton Trans.* **1991**, 497.

Table 8. Magnetic Parameters for the Cu^{II}M Complexes

complex		J, cm^{-1}	g_{Cu}	g_{M}	$\langle g \rangle$
1	Cu ^{II} Cr ^{III} (OCH ₃)	+18.5	2.03	2.00	
2	Cu ^{II} Mn ^{III} (OAc)	+54.4			2.02
3	Cu ^{II} Mn ^{II} (OAc)	-41.4			2.01
4	Cu ^{II} Fe ^{III} (Cl)	-38.8			2.00 (fixed)
4a	Cu ^{II} Fe ^{III} (OAc)	-44.9	2.03	1.91	
5a	Cu ^{II} Co ^{II} (OAc)	-53.8			2.41
6	Cu ^{II} Co ^{III} (Cl)	$\mu_{\text{eff}} = 1.86 \pm 0.03 \mu_{\text{B}}$ (81–293 K)			
7a	Cu ^{II} Ni ^{II} (OAc)	-99.2			2.25
8	Cu ^{II} Cu ^{II}	-298			2.01
9	Cu ^{II} Zn ^{II} (OH ₂)	$\mu_{\text{eff}} = 1.81 \pm 0.02 \mu_{\text{B}}$ (81–293 K)			

out using the Heisenberg–Dirac–van Vleck (HDvV) model^{31,32} as simplified to the isotropic Hamiltonian for the case of dimers $H = -2J\hat{S}_1\hat{S}_2$. A full-matrix diagonalization approach including magnetic exchange ($-2JS_1S_2$), Zeeman interactions, and axial single-ion zero-field interaction (DS_2^2), in case of necessity, was employed to fit the data (except for 4; see later). Table 8 summarizes intradimer exchange parameters together with other parameters.

In the range 81–293 K complexes 6 and 9 have essentially temperature-independent μ_{eff} values of 1.86 ± 0.03 and $1.81 \pm 0.02 \mu_{\text{B}}$, respectively. There is an unpaired electron localized on the Cu(II) center in 6 or 9, and the magnetic moment is expected to lie in the range 1.75–1.90 μ_{B} . This is a clear indication of the fact that we are dealing with genuine Cu^{II}Co^{III} 6 and Cu^{II}Zn^{II} 9, species with a low-spin diamagnetic d⁶ Co(III) ion and a diamagnetic d¹⁰ Zn(II) ion, respectively, in complete agreement with EPR results.

The μ_{eff} values for 8 vary only slightly over the temperature range from 1.02 μ_{B} at 303 K to 0.41 μ_{B} at 87 K, showing that the magnitude of the antiferromagnetic exchange integral between the cupric ions is very large. A least-squares fit with $2J = -596 \text{ cm}^{-1}$ can be obtained. This is in complete accord with the lack of EPR signals up to 50 K. We note that the coupling in a similar Cu^{II}Cu^{II} compound described in the literature²⁴ is stronger ($2J = -866 \text{ cm}^{-1}$) than that in 8.

The temperature dependence of the magnetic moments of 1–4 and 7a are displayed in Figure 7. The experimental magnetic moment for 7a decreases as the temperature is lowered until a plateau is reached at ~ 35 K with $\mu_{\text{eff}} = 1.952 \mu_{\text{B}}$, which is nearly the theoretical value of $\mu_{\text{eff}} = 1.949 \mu_{\text{B}}$ for an $S = 1/2$ ground state with $g = 2.25$, evaluated along with $2J = -198.4 \text{ cm}^{-1}$ from the least-squares fitting of the magnetic data (solid line in Figure 7). Thus, we conclude there is a moderately strong antiferromagnetic exchange interaction between Cu(II) and Ni(II) ions of complex 7a, with a resulting $S = 1/2$ ground state. Below 25 K with a μ_{eff} value of 1.932 μ_{B} there is a decrease in μ_{eff} reaching a value of 1.837 μ_{B} at 2 K. This deviation below ~ 25 K from the theoretical value of 1.949 μ_{B} may be the result of intermolecular antiferromagnetic interactions between neighboring dinuclear complexes.

Magnetic data for a polycrystalline sample of complex 4 were collected in the temperature range 4.2–284 K (Figure 7). At 284.5 K, the μ_{eff} value is 5.61 μ_{B} , which is much lower than the theoretical value $\mu_{\text{eff}} = 6.17 \mu_{\text{B}}$, expected for two noncoupled spins of $S_{\text{Cu}} = 1/2$ and $S_{\text{Fe}} = 5/2$. On lowering of the temperature, μ_{eff} decreases monotonically until a plateau is reached in the temperature range 25–85 K, with μ_{eff} values varying between 4.83 and 4.90 μ_{B} , very close to the spin-only value of $\mu_{\text{eff}} = 4.90 \mu_{\text{B}}$ for $S = 2$, expected as the ground state of an antiferromagnetically coupled Cu^{II}Fe^{III} complex. Below 20 K, there is a decrease in μ_{eff} reaching a value of 4.32 μ_{B} at 4.2 K. To fit the low-temperature ($T < 20$ K) data, it was necessary to consider

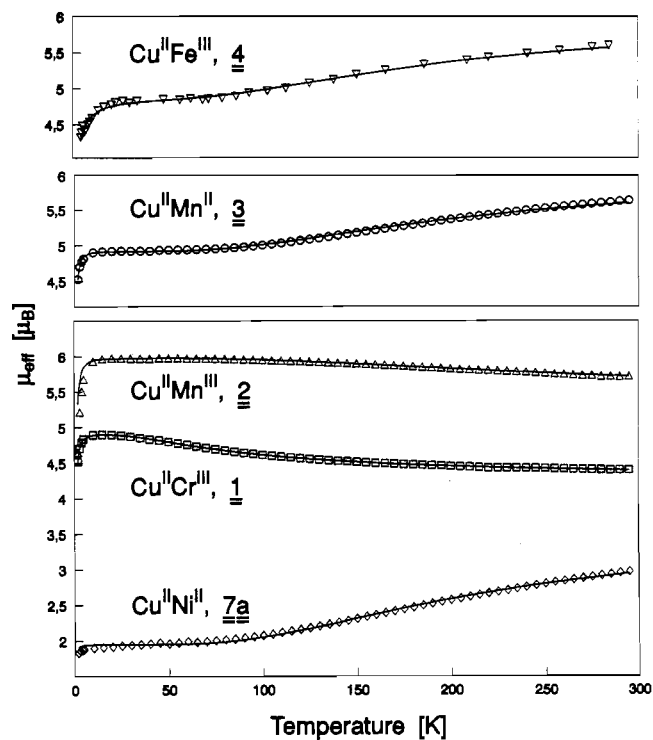


Figure 7. Plots of μ_{eff} vs temperature for 1–4 and 7a. The solid lines represent the best least-squares fit of the experimental data to the theoretical equations.

a constant Θ . The expression used is

$$\chi_{\text{calc}}^{\text{FeCu}} = \frac{C}{T - \Theta} f(J, T)$$

were $C = Ng^2\mu_{\text{B}}^2/k$ and $f(J, T)$ is derived from the theoretical equation. The experimental values have been fitted to this equation by treating the exchange interaction J and the Weiss constant Θ as adjustable parameters. The Zeeman interaction of the high-spin ferric ion in the 6A_1 ground state with practically no contribution from orbital angular momentum is isotropic; the observed g_{Fe} values are close to the free-electron spin value of 2.0. Hence we have fixed g to 2.0. The quality of the fit does not improve by allowing g to vary. Moreover, local g_{Fe} dominates over local g_{Cu} , as can be seen in the molecular g -tensor expressions^{2,25}

$$g_{S=2} = 7/6g_{\text{Fe}} - 1/6g_{\text{Cu}}$$

$$g_{S=3} = 5/6g_{\text{Fe}} + 1/6g_{\text{Cu}}$$

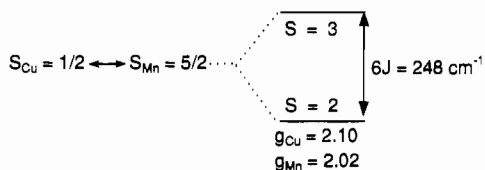
in determining the g values of complex 4, thus lending further support for fixing g at 2.0 in the fitting procedure. The best fit parameters are $2J = -77.6 \text{ cm}^{-1}$ and $\Theta = -1.25 \text{ K}$.

The experimental magnetic moment of 3 decreases as the temperature is lowered until a plateau is reached in the temperature range 10–75 K with μ_{eff} values lying between 4.902 and 4.954 μ_{B} , which are nearly the theoretical value of $\mu_{\text{eff}} = 4.923 \mu_{\text{B}}$ for an $S = 2$ ground state with $g = 2.01$, evaluated along with $2J = -82.8 \text{ cm}^{-1}$ from the least-squares fitting of the magnetic data (solid line in Figure 7). Thus, there is moderate antiferromagnetic exchange interaction between Cu(II) and Mn(II) ions in complex 3, with a resulting $S = 2$ ground state. Below 10 K with a μ_{eff} value of 4.902 μ_{B} there is a decrease in μ_{eff} reaching a value of 4.527 μ_{B} at 2 K. Using the g_{Cu} value of 2.10 obtained from the EPR data for 9, g_{Mn} can be easily calculated to be 2.02, which is in complete accord with the expected g value for a high-spin Mn(II) ion in a 6A_1 ground state. The following

(31) Ginsberg, A. P. *Inorg. Chim. Acta Rev.* 1971, 5, 45.

(32) (a) Goodenough, J. B. *Magnetism and the Chemical Bond*; Wiley: New York, 1963. (b) Anderson, P. W. *Phys. Rev.* 1959, 115, 2. (c) Anderson, P. W. In *Solid State Physics*; Seitz, F., Turnbull, D., Eds.; Academic Press: New York, 1963; p 99.

low-lying energy diagram appropriate for **3** is obtained from the magnetic studies:



The magnetic behavior of **2**, Cu^{II}Mn^{III}, is quite characteristic of a ferromagnetically coupled ion pair. At 295 K the μ_{eff} value is 5.716 μ_{B} , which is much higher than the theoretical value $\mu_{\text{eff}} = 5.248 \mu_{\text{B}}$ expected for two uncoupled spins of $S_{\text{Cu}} = 1/2$ and $S_{\text{Mn}} = 4/2$. On lowering of the temperature, μ_{eff} increases very slowly until it reaches a value of 5.976 μ_{B} at 25 K, which is exactly the spin-only value for $S = 5/2$ expected as the ground state for a ferromagnetically coupled Cu^{II}Mn^{III} complex. Below 25 K, there is a decrease in μ_{eff} reaching a value of 4.649 μ_{B} at 2 K, probably because of antiferromagnetic intermolecular spin coupling. The other μ_{eff} /per molecule values are 5.975, 5.968, 5.930, 5.679, 5.508, and 5.215 μ_{B} at 20, 15, 10, 5, 4, and 3 K, respectively. The interaction between the Mn(III) and Cu(II) ions gives rise to $S = 3/2$ and $S = 5/2$ pair states, with an energy gap of 5 J. The corresponding Zeeman factors $g_{3/2}$ and $g_{5/2}$ are related^{2,25} to the local Zeeman factors g_{Mn} and g_{Cu} through the following expressions:

$$g_{5/2} = 4/5 g_{\text{Mn}} + 1/5 g_{\text{Cu}}$$

$$g_{3/2} = 6/5 g_{\text{Mn}} - 1/5 g_{\text{Cu}}$$

Diagonalization of the Hamiltonian matrix yields $g = 2.02$ and $2J = +108.8 \text{ cm}^{-1}$. The solid line in Figure 7 shows the quality of the fit, which is reasonably good. The sextet–quartet energy gap is thus equal to $5J = 272 \text{ cm}^{-1}$. The g_{Mn} value deduced for **2** is found to be equal to 2.00, using the g_{Cu} value of 2.10 obtained for **9** from EPR measurements. An important point needs to be mentioned here. We found it necessary to prevent polycrystalline samples of **2** from partially torquing in the external field, in order to determine accurately the magnetic moments, particularly at low temperature. To this end, the polycrystalline samples of complex **2** were restrained from torquing either by embedding the sample in paraffin or by packing the powdered sample tightly in the sample holder. Both methods yielded same results. A similar dimethylglyoximate-bridged Cu^{II}Mn^{III} pair was recently reported,²⁹ but without an X-ray structure. The observed ferromagnetic coupling ($2J = +52 \text{ cm}^{-1}$) is much weaker than that in **2**.

At 295 K the magnetic moment, μ_{eff} /molecule for **1**, is 4.398 μ_{B} , which is slightly higher than the theoretical value of $\mu_{\text{eff}} = 4.239 \mu_{\text{B}}$ expected for two noncoupled spins of $S_{\text{Cu}} = 1/2$ and $S_{\text{Cr}} = 3/2$. On lowering of the temperature, μ_{eff} increases monotonically until a plateau is reached in the temperature range 10–25 K with a μ_{eff} value of 4.90 μ_{B} , which is the theoretical spin-only value for $S = 2$, expected as the ground state for a ferromagnetically coupled Cu^{II}Cr^{III} compound. Below 10 K, there is a decrease in μ_{eff} reaching a value of 4.521 μ_{B} at 2 K. This deviation below 10 K from the theoretical value of 4.90 μ_{B} may be due to the effect of weak antiferromagnetic intermolecular interactions between neighboring heterodinuclear complexes. The least-squares fitting, shown as the solid line in Figure 7, of the experimental data leads to $2J = +37 \text{ cm}^{-1}$, $g_{\text{Cu}} = 2.03$, and $g_{\text{Cr}} = 2.00$. The fitted g_{Cu} value for **1** is in conformity with the experimentally (EPR) obtained g_{Cu} values for **9**, Cu^{II}Zn^{II}, and for **6**, Cu^{II}Co^{III}. The g factors^{2,25} for the total spin states $S = 2$ and $S = 1$, g_2 and g_1 , respectively, are related to the local values

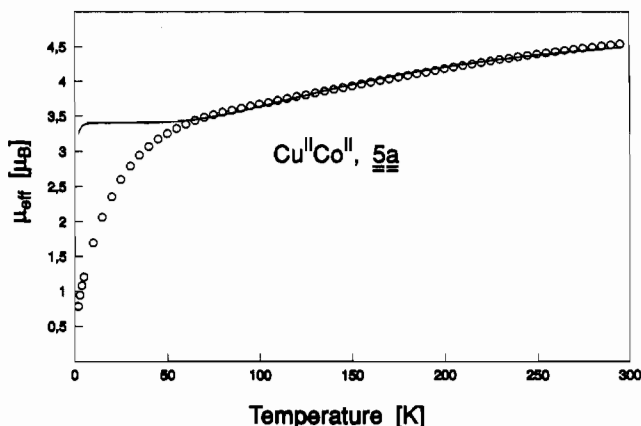


Figure 8. Effective magnetic moments μ_{eff} (O) as a function of temperature for **5a**. The solid line represents the simulation with $J = -53.8 \text{ cm}^{-1}$ and $g = 2.41$.

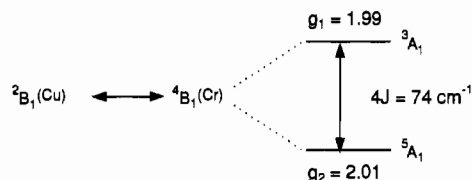
g_{Cu} and g_{Cr} by

$$g_1 = 5/4 g_{\text{Cr}} - 1/4 g_{\text{Cu}}$$

$$g_2 = 3/4 g_{\text{Cr}} + 1/4 g_{\text{Cu}}$$

The g values associated with the $S = 2$ and $S = 1$ states are thus found to be 2.01 and 1.99, respectively. A similar oximate-bridged Cu^{II}Cr^{III} dinuclear compound was recently reported,³⁰ but without an X-ray structural characterization. The observed ferromagnetic coupling ($2J = +25.2 \text{ cm}^{-1}$) is weaker than that in **1**.

It is noteworthy that in complexes **1**, **3**, **4**, and **4a** the ground states are spin quintets, $S = 2$. In **3**, **4**, and **4a**, $S = 2$ arises through an antiferromagnetic interaction between the local spin carriers; but in **1** a ferromagnetic interaction leads to the $S = 2$ ground state. The low-lying states for **1** are depicted as follows considering the idealized C_{2v} symmetry:



The cryomagnetic property of the Cu^{II}Co^{II} complex, **5a**, is shown in Figure 8 in the form of a μ_{eff} vs T plot. The magnetic moment of 4.537 μ_{B} at 295 K decreases steadily until at 50 K a μ_{eff} value of 3.250 μ_{B} is reached. Below 50 K, the magnetic moment decreases rapidly to a value of 0.779 μ_{B} at 2 K. The interpretation of the magnetic behavior of **5a** is complicated because of the unquenched orbital momentum of the Co(II) ion. The isotropic HDvV model is not strictly applicable^{26–28} for the estimation of exchange coupling, J , to octahedral Co(II) complexes since it ignores the effect of spin–orbit coupling within the ${}^4T_{1g}$ (F) ground term. The 4T_1 ground term for a Co(II) ion in an octahedral field yields ${}^4A_2 + {}^4B_1 + {}^4B_2$ terms in C_{2v} symmetry (idealized), each of them being split into two Kramers doublets by spin–orbit coupling. Our low-temperature (2–50 K) magnetic data for **5a** could not be fitted to the spin-only model, even taking into account the axial single-ion zero-field interaction (DS_z^2) of Co(II), showing the complexity of the cryomagnetic behavior. Particularly, the nearly diamagnetic behavior (0.78 μ_{B} at 2 K) of **5a** at very low temperature cannot be explained by considering only two spin states, $S = 1$ and $S = 2$ ($S_{\text{Cu}} = 1/2$, $S_{\text{Co}} = 3/2$) arising through the exchange interaction between the paramagnetic metal centers in the Cu^{II}Co^{II} complex, **5a**. By neglecting the single-ion terms in Hamiltonian arising from the orbital degeneracy of the Co(II) ion, it is totally impossible to interpret the magnetic

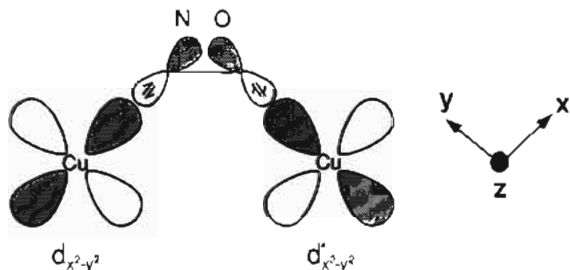
behavior of **5a** below 50 K, where spin-orbit coupling plays a dominant role. Considering only the data in the range 50–295 K, a fairly good simulation could be obtained with $2J = -107.6$ cm⁻¹ and $g = 2.41$ (Figure 8, solid line).

We wish to provide a qualitative rationale for the trend and the nature of exchange interactions between two spin carriers, Cu(II) and M. Although it is known from the literature²⁶ that the spin-only approach used here for the evaluation of J for **5a**, Cu^{II}Co^{II}, does yield, neglecting the very low temperature data where spin-orbit coupling plays a dominant role, a value of J that is not far from the real exchange coupling constant, we will not consider the compound **5a** in the following discussion.

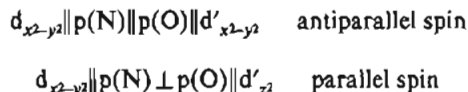
The sign of the intramolecular exchange coupling constants results from the sum of antiferromagnetic and ferromagnetic contributions:

$$J = J_{AF} + J_F \quad (1)$$

The environment around the copper(II) ions in complexes **1–9** is square pyramidal with ($d_{x^2-y^2}$) ground states. Thus the magnetic orbitals of Cu(II) ions, $d_{x^2-y^2}$, point from the metal toward the four nearest neighbors and overlap on either side of the bridging oximate ligand in **8**. The principal magnetic exchange pathway is considered to be of σ nature. Because of the symmetry properties of the σ interaction, $d_{x^2-y^2}$ orbitals on the Cu(II) ions and σ orbitals on the bridging oxygen and nitrogen atoms are involved in the exchange pathway for unpaired spin density. Thus the strong antiferromagnetic interaction in **8** (Table 8) can be interpreted as the symmetry-allowed $d_{x^2-y^2}||p(N)||p(O)||d'_{x^2-y^2}$ (using Ginsberg's symbols)³¹ σ -superexchange pathway. The following drawing shows the orientation of the relevant orbitals for the mechanism of interaction:



Now, going to the Cu^{II}Ni^{II} species, **7a** (d^9-d^8), the strength of overall antiferromagnetic interaction decreases drastically from -596 to -198.4 cm⁻¹. Two unpaired electrons in the e'_g orbitals of Ni(II), i.e. ($d_{x^2-y^2}$)¹(d_{z^2})¹, provide two exchange pathways:



The extra pathway in **7a** involving the d_{z^2} orbital of the Ni(II) center provides a ferromagnetic contribution to the overall magnetic interaction (eq 1), thus resulting in a reduction in the strength of the net antiferromagnetic spin coupling. The $J(d_{x^2-y^2}/d'_{x^2-y^2})$ path still dominates the overall interaction. Considering the energy difference δ between the magnetic orbitals of the two metal sites to be larger in **7a**, Cu^{II}Ni^{II}, than that in **8**, Cu^{II}Cu^{II}, it is expected that J_8/J_{7a} be significantly greater than 2. Our experimental value is consistent with this prediction.²⁸

We now consider the d^9-d^5 case (**3**, **4**, **4a**). There is again a further reduction in the antiferromagnetic interaction on going

from d^8 to d^5 in an octahedral environment. In this case also the sign of J is governed by the sign of J_{AF} in eq 1. The ferromagnetic contributions provided by the $d_{x^2-y^2}||p(N)\perp p(O)||t'_{2g}$ exchange paths cannot completely balance the dominant $d_{x^2-y^2}||p(O)||d'_{x^2-y^2}$ antiferromagnetic interaction, leading to an effective antiparallel spin coupling but much weaker than that in **7a**. On substitution of the Ni(II) ion by a d^5 Mn(II) or Fe(III) ion in an octahedral environment, the magnitude of the antiferromagnetic interaction is expected to decrease by a factor of 2.5. The factors found for **3**, **4**, and **4a** are 2.4, 2.6, and 2.2, respectively.

We now turn to the d^9 -h.s. d^4 and d^9-d^3 pairs. In **2**, the Mn(III) center (h.s. d^4) is tetragonally distorted with the electronic configuration of the localized metal orbitals being (d'_{y^2} , d'_{xz})², (d'_{xy})¹, (d'_{z^2})¹, ($d'_{x^2-y^2}$)⁰ in order of increasing energy. Thus the magnetic orbitals of the Mn(III) center are orthogonal to the $d_{x^2-y^2}$ orbital of the Cu(II) ion, resulting in parallel spin alignment (Goodenough-Kanamori rules).³² Similarly, the paths $d_{x^2-y^2}||p(N)\perp p(O)||t'_{2g}$, affording only positive terms in eq 1, lead to ferromagnetic interaction with an $S = 2$ ground state for **1**. The magnitude of the ferromagnetic interaction of **2**, Cu^{II}Mn^{III}, is expected to be greater than that for **1**, Cu^{II}Cr^{III}, owing to the additional path available in **2**, e.g. the interaction via the orthogonal path $d_{x^2-y^2}||p(N)\perp p(O)||d'_{z^2}$ of Cu^{II}Mn^{III}. This ferromagnetic interaction path is absent in **1**. Our experimental results confirm this expectation (Table 8).

From the expressions³ of J for **1** and **2**

$$J_{Cu^{II}Cr^{III}} = 1/6(J_{x^2-y^2,xy} + J_{x^2-y^2,yz} + J_{x^2-y^2,xz}) = 18.5 \text{ cm}^{-1}$$

$$J_{Cu^{II}Mn^{III}} = 1/6(J_{x^2-y^2,xy} + J_{x^2-y^2,yz} + J_{x^2-y^2,xz} + J_{x^2-y^2,z^2}) = 54.4 \text{ cm}^{-1}$$

a significantly larger value of ca. 320 cm⁻¹ could be evaluated for the ferromagnetic term $J_{x^2-y^2,z^2}$, indicating the importance of σ orbitals (note that $J_{x^2-y^2,x^2-y^2} = -298$ cm⁻¹, as obtained from **8**) in the magnetic exchange pathways for this family of compounds.

Concluding Remarks

The results described in the present paper show that the oximate dianion (Dopn²⁻) is capable of coordinating as a bridging ligand between two similar or dissimilar metal ions to give rise to various kinds of dinuclear complexes and, thus, can mediate a varying range of exchange interactions, weak, moderate to very strong antiferromagnetic and even ferromagnetic. Because of their quasi-isostructural nature, these materials are ideally suited for the study of intramolecular exchange interactions.

This paper confirms the essentially σ nature of the Cu(Dopn)-M interaction and the applicability of Goodenough-Kanamori rules, in general, to predict the nature of exchange interactions for different heterometal compounds. The strength of antiferromagnetic interaction decreases in the following order: Cu^{II}Cu^{II} > Cu^{II}Ni^{II} > Cu^{II}Co^{II} > Cu^{II}Mn^{II} ~ Cu^{II}Fe^{III}. The ferromagnetic interaction is stronger in Cu^{II}Mn^{III} than in Cu^{II}Cr^{III}.

This investigation also emphasizes the observation of well-resolved $S = 2$ EPR spectra for different heterometal systems.

Acknowledgment. Financial support from the DFG and the Fonds der Chemischen Industrie is gratefully acknowledged. Our thanks are also due to Prof. Dr. W. Haase and Dipl. Chem. C. Erasmus (Darmstadt) for the susceptibility measurements of **4**.

Supplementary Material Available: Tables of crystal data and intensity measurements, intraligand bond distances and angles, anisotropic thermal parameters, and hydrogen atom coordinates (14 pages). Ordering information is given on any current masthead page.